GEOSPHERE

GEOSPHERE, v. 18, no. 2

https://doi.org/10.1130/GES02448.1

11 figures; 4 tables; 1 supplemental file

CORRESPONDENCE: molnar@colorado.edu

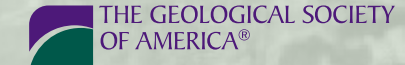
CITATION: Molnar, P., 2022, Differences between soil and air temperatures: Implications for geological reconstructions of past climate: Geosphere, v. 18, no. 2, p. 800–824, https://doi.org/10.1130/GES02448.1.

Science Editor: David E. Fastovsky Associate Editor: Andrew V. Zuza

Received 6 May 2021 Revision received 26 July 2021 Accepted 5 September 2021

Published online 4 February 2022





This paper is published under the terms of the CC-BY-NC license.

© 2022 The Author

Differences between soil and air temperatures: Implications for geological reconstructions of past climate

Peter Molnar

Department of Geological Sciences, Cooperative Institute for Research in Environmental Sciences (CIRES), University of Colorado at Boulder, Boulder, Colorado 80309-0399, USA

ABSTRACT

Among quantities of interest in paleoclimate, the mean annual air temperature, T_a, directly over the surface looms prominently. Most geologic estimates of past temperatures from continental regions, however, quantify temperatures of the soil or other material below the surface, T_{s} , and in general $T_a < T_s$. Both theory and data from the FLUXNET2015 data set of surface energy balance indicate systematic dependences of temperature differences $\Delta T = T_s - T_a$ and also of Bowen ratios—ratios of sensible to latent heat fluxes from surface to the atmosphere - on the nature of the land-surface cover. In cold regions, with mean annual temperatures ≤5 °C, latent heat flux tends to be small, and values of ΔT can be large, 3-5 °C or larger. Over wet surfaces, latent heat fluxes dominate sensible heat fluxes, and values of both ΔT and Bowen ratios commonly are small. By contrast, over arid surfaces that provide only limited moisture to the overlying atmosphere, the opposite holds. Both theory and observation suggest the following, albeit approximate, mean annual values of ΔT : for wetlands, 1 °C; forests, 1 ± 1 °C; shrublands, 3–4 °C; savannas, 3.5 °C $< \Delta T <$ 5.5 °C; grasslands, 1 °C where wet to 3 °C where arid; and deserts, 4-6 °C. As geological tools for inferring past land-surface conditions improve, these approximate values of ΔT will allow geologic estimates of past mean annual surface temperatures, T_s , to be translated into estimates of past mean annual air temperatures, T_a .

■ INTRODUCTION

Anyone who has walked barefoot on concrete surrounding a swimming pool on a hot, sunny summer day knows that the ground surface can be much hotter than the air immediately above it. Insolation impinging on the bare concrete surface heats that surface and creates an extreme difference between the temperature of the surface, $T_{\rm s}$, and that of the overlying air, $T_{\rm a}$. In other settings, differences between them, $\Delta T = T_{\rm s} - T_{\rm a}$, can range from negligible and even negative values to several degrees Celsius. Geologic materials commonly yield estimates of temperatures, $T_{\rm s}$, in soils or other kinds of sediment or rock near the surface, but paleoclimatic studies rely on air temperatures, $T_{\rm a}$. Thus, some problems in paleoclimate become poorly constrained, if not intractable,

Peter Molnar https://orcid.org/0000-0002-3523-9172

without protocols for correcting geologic estimates of surface temperatures, $T_{\rm s}$, to air temperatures, $T_{\rm a}$. Although ignorance of ΔT adds a relatively small error to estimates of temperature differences between present-day and past temperatures at high latitudes or to temperature differences between sites at high and low elevations, values of ΔT are comparable to changes over geologic time in tropical and subtropical environments. For example, although many estimates of high-latitude Pliocene temperatures exceed those today by many degrees Celsius, to as much as ~10 °C, changes in tropical temperatures since Pliocene time could be negligible, or at most only ~1–2 °C; differences between inferences of $T_{\rm s}$ in Pliocene time and those today would be comparable to the uncertainties in ΔT and therefore to possible changes in $T_{\rm s}$.

The $21^{\rm st}$ century has brought us geologic methods for quantifying surface temperatures, $T_{\rm s}$. In one case, the clumping of carbon $^{13}{\rm C}$ and oxygen $^{18}{\rm O}$ in carbonate sediment, when reduced to molecules of ${\rm CO}_2$ with atomic mass of 47 (Δ_{47}), depends inversely on the square of the temperature at the time of carbonate formation (e.g., Eiler, 2007; Ghosh et al., 2006a, 2006b; Kelson et al., 2020; Quade et al., 2007, 2013). In another case, the number of branches in branched glycerol dialkyl glycerol tetraethers (brGDGTs), long carbon-chained lipids that are produced by bacteria living in soils, depends on temperature (e.g., De Jonge et al., 2014; Hopmans et al., 2004; Weijers et al., 2007). Although initial calibrations of both clumped isotopes and brGDGTs were made with air temperatures, $T_{\rm a}$, both obviously sense soil, not air, temperatures. Therefore, differences between $T_{\rm a}$ and $T_{\rm s}$ contribute scatter to such calibrations.

With much remaining to be done to understand not only which among seasonally varying temperatures the clumped isotopes and brGDGTs record but also the other conditions that introduce biases in inferred temperatures, I consider only mean annual temperatures here, but obviously, when seasonal dependences of paleothermometers are better understood and the factors that affect them can be detected in the geologic record, shorter durations and seasonal variations in ΔT should be considered.

Values of ΔT , at least when measured for summer or other warm intervals, differ for different surface conditions, with relatively large values over deserts and smaller ones over moist environments, and with differences with latitude (e.g., Burgener et al., 2019; Gallagher et al., 2019; Kelson et al., 2020; Lu et al., 2019; Passey et al., 2010; Wang et al., 2020). For example, Lu et al. (2019, their supplementary figure 3) reported average temperature differences between March and November ranging from ~1 °C for "forest," to ~1.5 °C for "woodland," to ~2.5 °C for "grassland," and to ~4.5 °C for "desert" environments. Gallagher

et al. (2019) pointed out that when mean annual precipitation does not exceed 300 mm, values of ΔT in summer could exceed 4 °C, but commonly were smaller where more precipitation fell. Similarly, Burgener et al. (2019) reported that only for regions with mean annual precipitation <600 mm/yr does ΔT in the hottest summer month exceed 4 °C and only in those cases where vegetation cover is sparse. In following sections, I offer theoretical arguments and measurements of ΔT that concur with these observations and will help guide the assignment of values of ΔT for past environments.

The discussion of basic theory is meant to be elementary and comprehensible to geologists with an understanding of basic physics but untrained in meteorology. For data pertinent to quantification of temperature differences ΔT , the FLUXNET data set (e.g., Baldocchi et al., 2001; Pastorello et al., 2020; Wilson et al., 2002) includes not only measurements of T_s and T_a but also measurements of sensible and latent heat fluxes that rely on eddy covariance techniques over surfaces with different types of land-surface cover. (This data set also includes measurements of rates at which water, CO2, and in some cases other gases are exchanged between the surface and atmosphere.) In a recent version, the FLUXNET2015 data set (Pastorello et al., 2020) includes measurements from 212 sites around the globe, and for most sites, measurements of T_s and T_a are part of this data set. Although the FLUXNET2015 data set reports measurements averaged over half-hourly, hourly, daily, and monthly intervals, for reasons noted above and discussed further below, I consider only annual average values. The FLUXNET2015 data set also reports the land cover of sites following the International Geosphere-Biosphere Programme (IGBP) land cover classification scheme, with 17 categories, but I consider only some

of them here (Table 1). My focus on geological environments limits analysis to sites covered by natural vegetation, and hence I exclude those classified as "Croplands" as well as those from urban environments or covered by ice or snow (Table 1). Unfortunately, the FLUXNET2015 data set includes no sites from deserts.

Surface temperatures are a widely used tool in paleoaltimetry, and some measurements show a dependence of ΔT on elevation (e.g., Pérez-Angel et al., 2020; Wang and Liu, 2021). Appendix B presents a brief theoretical discussion of how ΔT might vary with altitude in different settings.

Elementary Background on Clumped Isotopes, brGDGTs, and Soil Temperatures

Initial calibrations of clumped isotopes and brGDGTs commonly addressed mean annual air temperature, MAT (e.g., De Jonge et al., 2014; Eiler, 2007; Ghosh et al., 2006a, 2006b; Hopmans et al., 2004; Pérez-Angel et al., 2020; Quade et al., 2007; Russell et al., 2018; Weijers et al., 2007). A focus on MAT as well as on mean annual soil temperature (MAST) carries risks because even ignoring differences between T_a and T_s that depend on local environments, seasonal cycles in both precipitation and temperature can bias estimates of past temperatures. Several studies (Breecker et al., 2009; Burgener et al., 2016; Passey et al., 2010; Quade et al., 2013; Ringham et al., 2016) have shown that that pedogenic carbonates tend to form in warm, dry seasons and not necessarily during growth season of vegetation, though Breecker et al. (2009,

TABLE 1. THE INTERNATIONAL GEOSPHERE-BIOSPHERE PROGRAMME (IGBP) LAND-COVER CLASSIFICATION

	IADLE I	. THE INTERNATIONAL GEOSPHERE-BIOSPHERE PROGRAMME (IGBP) LAND-COVER CLASSIFICATION			
Class	Class name	Description			
1	Evergreen needleleaf forests	Lands dominated by needleleaf woody vegetation with a percent cover >60% and height exceeding 2 m. Almost all trees remain green all year. Canopy is never without green foliage.			
2	Evergreen broadleaf forests	Lands dominated by broadleaf woody vegetation with a percent cover >60% and height exceeding 2 m. Almost all trees and shrubs remain green year round. Canopy is never without green foliage.			
3	Deciduous needleleaf forests	Lands dominated by woody vegetation with a percent cover >60% and height exceeding 2 m. Consists of seasonal needleleaf tree communities with an annual cycle of leaf-on and leaf-off periods.			
4	Deciduous broadleaf forests	Lands dominated by woody vegetation with a percent cover >60% and height exceeding 2 m. Consists of broadleaf tree communities with an annual cycle of leaf-on and leaf-off periods.			
5	Mixed forests	Lands dominated by trees with a percent cover >60% and height exceeding 2 m. Consists of tree communities with interspersed mixtures or mosaics of the other four forest types. None of the forest types exceeds 60% of the landscape.			
6	Closed shrublands	Lands with woody vegetation less than 2 m tall and with shrub canopy cover >60%. The shrub foliage can be either evergreen or deciduous.			
7	Open shrublands	Lands with woody vegetation less than 2 m tall and with shrub canopy cover between 10% and 60%. The shrub foliage can be either evergreen or deciduous.			
8	Woody savannas	Lands with herbaceous and other understory systems and with forest canopy cover between 30% and 60%. The forest cover height exceeds 2 m.			
9	Savannas	Lands with herbaceous and other understory systems and with forest canopy cover between 10% and 30%. The forest cover height exceeds 2 m.			
10	Grasslands	Lands with herbaceous types of cover. Tree and shrub cover is less than 10%.			
11	Permanent wetlands	Lands with a permanent mixture of water and herbaceous or woody vegetation. The vegetation can be present either in salt, brackish, or fresh water.			

p. 639) noted that "carbonate formation can occur whenever the soil solution becomes supersaturated, which may occur at different times of year in different climates." More recent work has emphasized the importance of moisture and its variations in time, given that moisture brings CO₂ to the soil and then evaporation enables that CO₂ to concentrate in the carbonate (e.g., Gallagher and Sheldon, 2016). Moreover, because carbonate, like CaCO₃, is more soluble in cold than warm water, warm seasons are favored over cold ones for carbonate formation (e.g., Breecker et al. 2009; Gallagher and Sheldon, 2016). Thus, the timing of precipitation also influences the timing of carbonate formation (e.g., Gallagher and Sheldon, 2016; Huth et al., 2019; Peters et al., 2013).

Consistent with carbonates forming in warm seasons, estimates of temperatures from clumping of isotopes tend to be higher than MATs from sites with carbonates used for clumped-isotope analysis (e.g., Breecker et al., 2009; Burgener et al., 2016; Gallagher et al., 2019; Hough et al., 2014; Kelson et al., 2020; Passey et al., 2010; Peters et al., 2013; Quade et al., 2013; Ringham et al., 2016; Snell et al., 2013), although enough exceptions continue to invite further analysis (e.g., Gallagher and Sheldon, 2016; Kelson et al., 2020). In a recent review, Kelson et al. (2020) showed that temperatures, $\mathcal{T}(\Delta_{47})$, inferred from clumped isotopes, Δ_{47} , exceed MATs by ~10 ± 5 °C. Accordingly, most have treated temperatures estimated from clumped isotopes in carbonates as biased toward summer conditions (e.g., Hough et al., 2014; Quade et al., 2013; Passey et al., 2010; Peters et al., 2013; Snell et al., 2013), particularly in regions where temperatures drop below freezing for part of the year (Burgener et al., 2016, 2018). Even the nature of sediment in which carbonates form, cobbles versus sand, can affect inferences of temperatures based on clumped isotopes, at least in cold environments (Burgener et al., 2018). In their summary, Kelson et al. (2020, p. 14) stated: "For paleoclimate purposes, our analysis suggests that at this point in time $[\mathcal{T}(\Delta_{47})]$ does not represent an easily defined climate parameter such as mean summer temperature or peak summer temperature." Quade et al. (2013) had found that although temperatures inferred from clumped isotopes, $\mathcal{T}(\Delta_{47})$, exceeded mean annual air temperatures by much more than likely differences between T_a and T_s , a linear scaling of $T(\Delta_{47})$ and MAT works well.

Similarly, although brGDGTs are not yet studied in the same detail as clumped isotopes, Wang et al. (2016) and Lu et al. (2019) suggested that the bacteria responsible for the brGDGTs were most productive during the growing season of vegetation and presumably bacteria.

Depth Dependence of Seasonal Variations in Temperature in Soil

As is known well and shown by many of the studies mentioned above, the amplitude of temperature variations in soils associated with seasonal (and diurnal) cycles decays exponentially with depth. For temperature at the surface, depth z=0, varying sinusoidally with time, t: $T(z=0,t)=\delta T\sin(2\pi t't_0)$, and therefore with amplitude δT and period t_0 , temperature at depth is given by:

$$T(z,t) = \delta T \sin\left(\frac{2\pi t}{t_0} - \frac{z}{z_0}\right) e^{-\frac{z}{z_0}},\tag{1}$$

where $z_0 = \sqrt{\kappa t_0 / \pi}$ and κ is thermal diffusivity (e.g., Anderson, 1998; Anderson, son and Anderson, 2010, p. 275-276; Quade et al., 2013). For a seasonal cycle with a period, t_0 , of one year and $\kappa = 1-10 \times 10^{-7}$ m²/s appropriate for soils of different compositions and saturated to varying degrees (Al Nakshabandi and Kohnke, 1965), $z_0 = 1.0-3.2$ m. Soil carbonates or brGDGTs in bacteria at a depth of z_0 would experience a seasonally varying surface temperature 2.7 times smaller than the corresponding value at the surface (Fig. 1). If soil carbonates formed or bacteria lived sufficiently deep, they would not detect seasonal cycles in surface temperature. Accordingly, ignorance of the depths and soil saturation at which carbonates formed or bacteria lived complicates the interpretation of such paleotemperatures. In fact, in their compilation of values of values of $T(\Delta_{47})$ versus depth, Kelson et al. (2020) found no variation with depth. They suggested a couple of possible explanations for what they treated as a surprising coincidence, but the lack of variation in $\mathcal{T}(\Delta_{47})$ is consistent with Δ_{47} being calibrated to a quantity that scales with but is systematically offset from the MAT.

My focus is on soil, not lacustrine deposits, for which the relationship to subbottom temperatures in lakes to air temperatures above is yet more complicated. Nevertheless, for lacustrine sediment, a seasonal dependence seems to be constrained well. Huntington et al. (2010) found clumped isotopes in carbonates deposited in lake sediment to reflect summer temperatures.

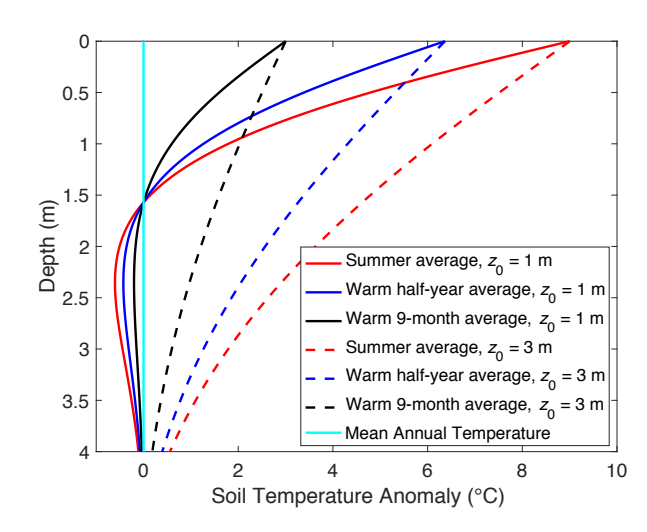


Figure 1. Profiles of temperature anomalies through soil for different periods of time, for a seasonal cycle of temperature varying from +10 °C in summer to -10 °C in winter about a mean annual value given by the cyan line. Curves are shown for averages over three periods: three summer months (red), the warm half of the year (blue), and the warmest ninemonth period (black), and for two scaling depths, z_0 , in Equation 1 that bound commonly inferred values for z_0 (Al Nakshabandi and Kohnke, 1965).

Similarly, several report that brGDGTs in lakes record temperatures above freezing (e.g., Dang et al., 2018; Martínez-Sosa et al., 2021; Raberg et al., 2021; Wang et al., 2021). brGDGTs that accumulate in sediment in lakes, however, bring the additional complication that some are produced by bacteria in the lake column and some are washed in from surrounding soils (e.g., Colcord et al., 2015; Günther et al., 2014; Li et al., 2016, 2017; Loomis et al., 2011; Russell et al., 2018; Tierney and Russell, 2009; van Bree et al., 2020; Wang et al., 2012; Weber et al., 2015). Separating the role played by each remains a challenge.

BASIC THEORY

In general, $T_{\rm s} > T_{\rm a}$ because of the balance of energy fluxes at the earth's surface. Both shortwave insolation, $Q_{\rm SW}$, and longwave radiation from greenhouse gases, $Q_{\rm LWghg}$, warm the surface (Fig. 2). The surface radiates some, commonly most, of that incoming radiation back to the atmosphere at long wavelengths, $Q_{\rm LW}$. Turbulent interactions between air and the underlying surface transfer the rest of the energy that has been absorbed by the surface back to the overlying atmosphere by surface enthalpy fluxes—sensible heat, SH, and latent heat, LH, fluxes (Fig. 2). Because greenhouse gases in the atmosphere absorb and then reradiate longwave radiation equally both upward and downward but the surface radiates only upward, the surface tends to be warmer on average, but not everywhere and not at all times, than the air immediately above it. Energy balance at the surface, averaged over periods long enough that there be no net storage of energy, requires (Fig. 2):

$$Q_{SW} + Q_{LWghg} = Q_{LW} + SH + LH.$$
 (2)

The balance in Equation 2 does not apply over the diurnal cycle because the earth's surface can store energy obtained during the day and lose it at night. Moreover, $Q_{\rm SW}$ varies over the seasonal cycle and, therefore, so do the other fluxes in Equation 2, but over longer times, and on geologic time scales, these fluxes balance.

Surface Energy Fluxes

Mean annual shortwave radiation from the sun, S_{\odot} , decreases with latitude. Reflection back into space by both clouds and the surface, which is parameterized by albedo, α , reduces the shortwave energy reaching the surface to be:

$$Q_{SW} = S_{\odot}(1 - \alpha). \tag{3}$$

Typical values of albedo range between 0.1 and 0.3 (e.g., Donohoe and Battisti, 2011). Annual average values of S_{\odot} vary with latitude, from ~420 W/m² at the equator, and if within ~60° of the equator, they are approximately proportional to the cosine of latitude (Fig. 3). Although $Q_{\rm SW}$ varies markedly both over the diurnal cycle and on seasonal time scales, it can be treated like all terms in Equation 2 as an annual average.

Both $Q_{\rm LWghg}$ and $Q_{\rm LW}$ in Equation 2 obey the Stefan-Boltzmann equation for black-body radiation but with different values of emissivity (and absorptivity), e, a factor between 0 and 1 that takes into account deviations from strictly black bodies:

$$Q_{LW} = e_s \sigma T_s^4$$
 and $Q_{LWghg} = e_s e_a \sigma T_a^4$, (4)

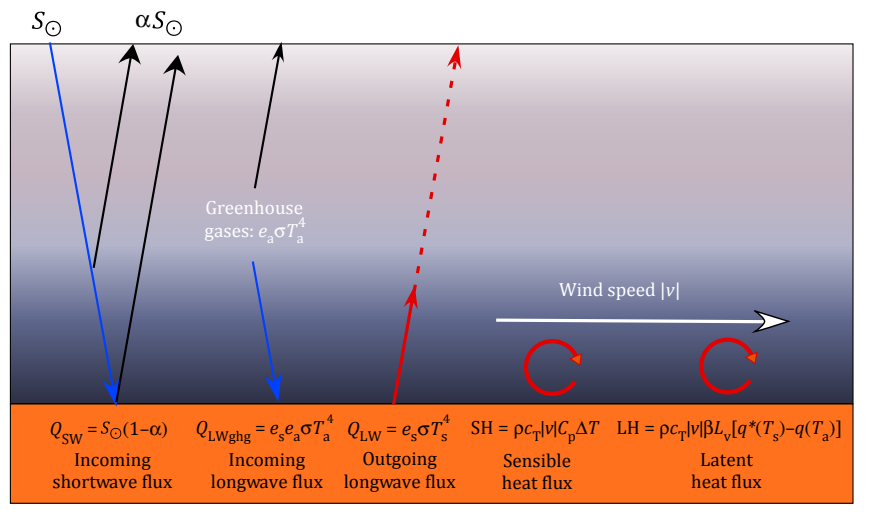


Figure 2. Surface energy budget, including all terms in (2). The surface receives a fraction of shortwave energy, S_{\odot} , radiated by the sun, $Q_{SW} = S_{\odot}$ ($1-\alpha$), where α is the albedo; a fraction is reflected back to space, αS_{\odot} . The surface also receives longwave energy radiated both downward and upward by the atmosphere, largely by greenhouse gases in it, Q_{LWghg} , given by (4). The surface transfers energy upward to the atmosphere both by longwave radiation, Q_{LW} also given by Equation 4, some of which is absorbed by the atmosphere and some continues to space, and by mechanical or turbulent processes: sensible heat flux, SH, given by Equation 7, and latent heat flux, LH, given by Equation 8.

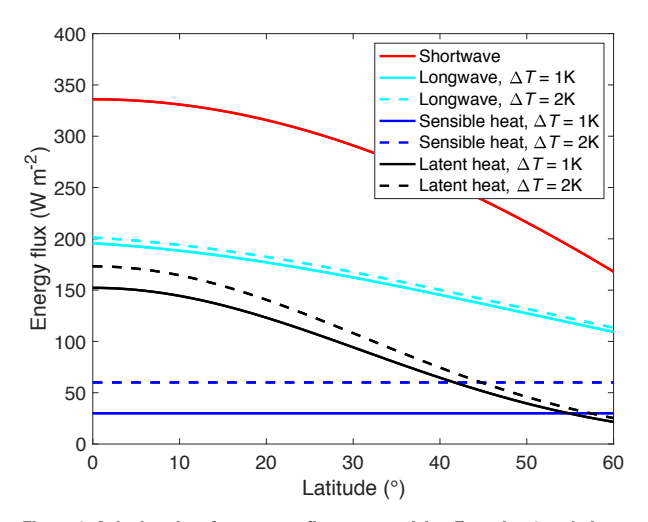


Figure 3. Calculated surface energy fluxes comprising Equation 2 and given by Equations 3, 5, 7, and 9 versus latitude, for which the mean annual air temperature, MAT, or T_{ar} the temperature of the air just above the surface, obeys an approximate form: $T_{a}(K)=240+60\cos\phi$, where ϕ is latitude, the moisture availability $\beta=0.2$, and the relative humidity RH = 0.6. With T_{s} equal to the temperature of soil, solid and dashed lines distinguish values of $\Delta T=T_{s}-T_{a}=1$ K from $\Delta T=2$ K.

where $\sigma=5.67\times 10^{-8}$ W/m²/K⁴ is the Stefan-Boltzmann constant, $e_{\rm s}$ and $e_{\rm a}$ are values of emissivity at the ground surface and in the overlying air at an appropriate height that depends on the optical thickness of the atmosphere, respectively, and $T_{\rm s}$ and $T_{\rm a}$ are expressed in kelvins. The product $e_{\rm s}e_{\rm a}$ in the expression for $Q_{\rm LWghg}$ arises because the atmosphere with its greenhouse gases radiates longwave radiation proportional to emissivity $e_{\rm a}$, and the surface then absorbs that flux proportional to its absorptivity $e_{\rm s}$. In an optically thin atmosphere, there is little absorption of radiation, and $e_{\rm a} \rightarrow 0$ (the arrow indicates "approaches"), but as the optical thickness increases, $e_{\rm a} \rightarrow 1$ (e.g., Pierrehumbert, 2010, p. 388–399). In general, $e_{\rm s} \lesssim 0.9$, but $e_{\rm a}$ and the resulting optical thickness decrease with temperature because the amount of water vapor decreases with temperature (e.g., Pierrehumbert, 2010, p. 388–391). The net longwave radiation from the surface, therefore, is the difference between $Q_{\rm LW}$ and $Q_{\rm LWghg}$ (Fig. 2).

The difference between Q_{LW} and Q_{LWaha} can be written as:

$$Q_{LW} - Q_{LWahg} = e_s \sigma \left(T_s^4 - e_a T_a^4 \right). \tag{5}$$

The combination of the fourth-power dependences on temperatures, typical values of $T_{\rm s} > T_{\rm a}$, and the decrease of $e_{\rm a}$ with temperature make the difference between $Q_{\rm LW}$ and $Q_{\rm LWaha}$ also decrease with temperature, and with latitude

because the MAT decreases with latitude (Fig. 3). Following Pierrehumbert (2010, p. 389), because $\Delta T = T_{\rm s} - T_{\rm a}$ is small compared with either $T_{\rm s}$ or $T_{\rm a}$, Equation 5 can be linearized:

$$Q_{LW} - Q_{LWaha} = e_s e * \sigma T_a^4 + 4e_s \sigma T_a^3 \Delta T, \tag{6}$$

where $e^* = (1 - e_a)$. Pierrehumbert (2010, p. 390) showed that for typical Cenozoic concentrations of CO_2 , which affect the concentration of H_2O in the atmosphere, e^* varies from ~0.4 at ~278 K (5 °C) to ~0.16 at 298 K (25 °C), though assigning an uncertainty to e^* is difficult.

Sensible heat flux, SH, is given by:

$$SH = \rho c_{T} |v| C_{D} (T_{S} - T_{A}) = \rho c_{T} |v| C_{D} \Delta T, \tag{7}$$

where ρ (= 1.2 kg/m³ at sea level) is the density of the air, C_p = 1000 J/kg/K is the specific heat of air at constant pressure, $c_T \approx 10^{-2}$ is a dimensionless enthalpy flux coefficient that increases weakly with wind speed, and |v| is the surface wind speed (e.g., Betts, 2000; Cronin, 2013; Pierrehumbert, 2010, p. 396). Pierrehumbert (2010, p. 395–402) explained the physics underlying Equation 7.

The latent heat flux can be expressed in different ways, but a common version is:

$$LH = \rho c_{T} |v| \beta L_{v} \left[q * (T_{s}) - q(T_{a}) \right], \tag{8}$$

where β is "moisture availability" (e.g., Betts, 2000; Cronin, 2013) and can range from $\beta \to 0$ in extreme desert conditions to $\beta \to 1$ over open water, $L_{\rm v} = 2.5 \times 10^6$ J/kg is the latent heat of vaporization, $q^*(T_{\rm s})$ is the specific humidity at saturation of moisture in the soil at temperature $T_{\rm s}$ (in kelvins), and $q(T_{\rm a})$ is the specific humidity of the overlying air at temperature $T_{\rm a}$ (in kelvins). Specific humidity is the fraction of water vapor in the air, and $q(T_{\rm a})$ can be written as the product of relative humidity, RH, and specific humidity of the air at saturation, $q^*(T_{\rm a})$: $q(T_{\rm a}) = {\rm RH} q^*(T_{\rm a})$. Below, I discuss how moisture availability β both depends on vegetation and differs in different settings. As discussed in Appendix A, because ΔT is small compared with $T_{\rm a}$ and $T_{\rm s}$, $q^*(T_{\rm s}) = q^*(T_{\rm a} + \Delta T)$ can be linearized around $T_{\rm a}$ to yield:

$$LH = \rho c_{\tau} |v| \beta L_{\nu} q^{*}(T_{o}) [1 + 0.07 \Delta T - RH], \tag{9}$$

where the factor 0.07 has implicit dimensions of K⁻¹ (or °C⁻¹). Latent heat flux decreases with decreasing temperature, and with increasing latitude (Fig. 3) because of the marked decrease of specific humidity at saturation, $q^*(T_a)$, with decreasing temperature, T_a , shown by Equations A3 and A4 in Appendix A.

Following Pierrehumbert (2010, p. 389, 392, and 399), by defining $b_{\rm ir}=4e_{\rm S}\sigma T_{\rm a}^3$, $b_{\rm sens}=\rho c_{\rm T}|v|C_{\rm p}$, and $b_{\rm lat}=0.07\rho c_{\rm T}|v|\beta L_{\rm v}q^*(T_{\rm a})$, inserting Equations 3, 6, 7, and 9 into Equation 2 yields:

$$S_{\odot}(1-\alpha) = e_{s}e * \sigma T_{a}^{4} + b_{ir}\Delta T + b_{sens}\Delta T + \rho c_{T}|\mathbf{v}|\beta L_{\nu}q * (T_{a})[1-RH] + b_{lat}\Delta T.$$
 (10)

Collecting terms yields:

$$\Delta T = \frac{S_{\odot}(1-\alpha) - e_{s}e^{*}\sigma T_{a}^{4} - \rho c_{T}|v|\beta L_{v}q^{*}(T_{a})[1-RH]}{b_{ir} + b_{sens} + b_{lat}}.$$
(11)

All three terms in the denominator are positive. As examples, for $T_a = 278$ K or 298 K: (1) with $e_s = 0.9$, $b_{ir} = 4.4$ or 5.4 W/m²/K; (2) with |v| = 2.5 m/s, $b_{sens} = 30$ W/m²/K; and (3) with $\beta = 0.2$, $b_{lat} = 5.6$ W/m²/K or 20.9 W/m²/K.

Some Basic Generalities of Surface Energy Fluxes

To illustrate how ΔT given by Equation 11 depends on some of the more important parameters, Figure 4 shows plots of ΔT versus air temperature T_a for two values of S_{\odot} (1 – α) = 336 and 168 W/m² appropriate for latitudes of 0° and 60°, respectively, and with α = 0.2 and |v| = 2.5 m/s, and (1) for different values of β = 0.1, 0.2, and 0.4 (e.g., Betts, 2000) with RH = 0.5 (Fig. 4A), and (2) for different values of RH = 0.3, 0.5, and 0.7 with β = 0.2 (Fig. 4B). Calculated values of ΔT decrease with T_a , largely because with increasing temperature, $q^*(T_a)$ increases but also because the second term in the numerator of Equation 11, due to black-body radiation, also increases with temperature. The increase of $q^*(T_a)$ with T_a leads both to decreases in the numerator of Equation 11 through the increase in its third term (latent heat flux) and to increases in the denominator, largely via b_{lat} , by somewhat less than a factor of two going from T_a = 0 °C to 30 °C. Because low temperatures, e.g., $T_a \lesssim 10$ °C, are unlikely

near the equator, the large values of ΔT for low latitudes are not applicable to present-day Earth-like conditions, and similarly, at 60° latitudes, we do not expect mean annual values of $T_a \gtrsim 20$ °C. Thus, the low- T_a side of the blue curves and the high- T_a side of the red curves in Figure 4 are most applicable.

From another perspective, where moisture is scarce and β is small, the surface enthalpy flux, SH + LH, must consist largely of sensible heat transfer. It follows that ΔT tends to be greater than where surface moisture is available (Fig. 4A). Similarly, as expected from Equation 11, a decrease in relative humidity of the air, RH, facilitates greater latent heat transfer at the expense of sensible heat transfer and leads to smaller values of ΔT than for large values of RH (Fig. 4B). This might seem counterintuitive, given the expectation of large values of ΔT in arid climates, but as discussed further below, the role of aridity manifests itself more in moisture availability, β , than in relative humidity, RH.

Bowen Ratio: Latent and Sensible Heat Flux

As discussed above, ΔT depends to a large extent of the degree to which surface enthalpy fluxes are partitioned into sensible heat, which is proportional to ΔT , and latent heat, which depends only weakly on ΔT . The Bowen ratio, B, is the ratio of sensible heat flux, SH, to latent heat flux, LH:

$$B = \frac{SH}{LH} = \frac{C_{p}\Delta T}{\beta L_{\nu} q^{*}(T_{a})(1 + 0.07\Delta T - RH)}.$$
 (12)

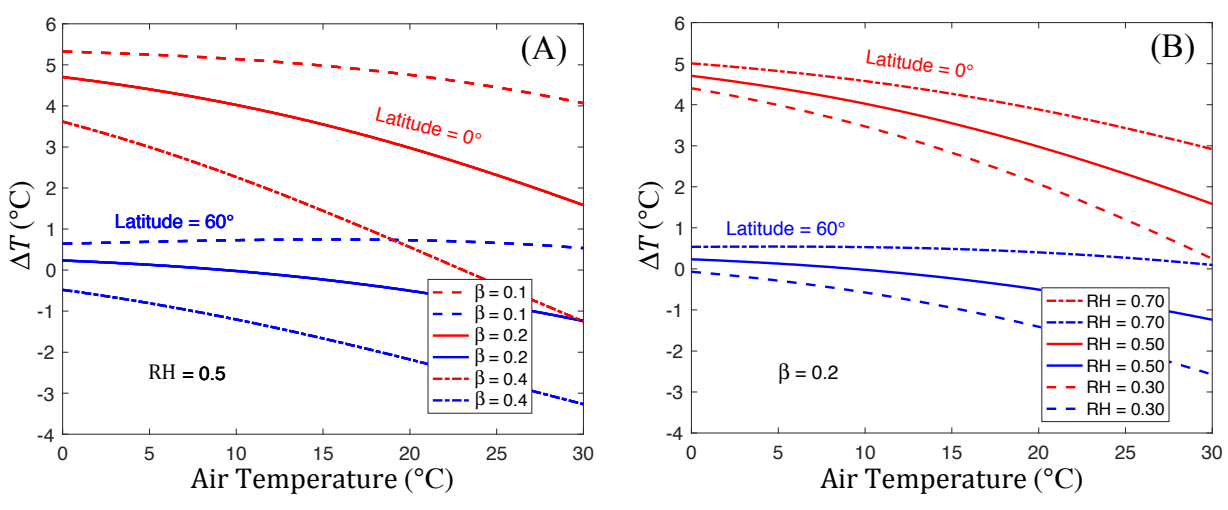


Figure 4. Calculated values of ΔT , the difference between soil temperature T_s , and that of the overlying air, T_a , from Equation 11 as a function of T_a or using the mean annual temperature MAT = T_a for two values of S_{\odot} (1 – α) = 336 W/m² (low latitude, 0°) and 168 W/m² (high latitude, 60°), and with |v| = 2.5 m/s, where S_{\odot} is the incident shortwave energy at the topo the atmosphere, α is albedo, and the average wind speed at the surface |v|. (A) ΔT for different values of moisture availability, β , with relative humidity, RH, = 0.5. (B) ΔT for different values of RH with β = 0.2.

The dependence of both SH and LH on $\rho c_T |v|$ cancels out in B. Because in general, if not everywhere, ΔT is only a few degrees Celsius, B is approximately proportional to ΔT but depends strongly on β and on T_a via $q^*(T_a)$. Thus, differences in values of B can provide insights into differences in ΔT . As Equation 12 shows, B should increase almost linearly with ΔT and decrease inversely with β (Fig. 5). The minor effect of ΔT on LH through the term $0.07\Delta T$ in the denominator of B can be seen by comparing the nearly identical values of B (1) for $\Delta T = 1$ °C and $\beta = 0.2$ and (2) for $\Delta T = 2$ °C and $\beta = 0.4$ (Fig. 5).

Moisture Availability, β , and Resistance to (or Conductance of) Moisture by Different Land-Surface Cover

With a focus on how ΔT and B depend on land-surface cover, key quantities are the ingredients of moisture availability, β . As noted above, for a lake or ocean, there is virtually no limit to the availability of moisture and $\beta \approx 1$, but over land, the surface is rarely so saturated. In addition to the transfer of moisture from the soil to the atmosphere, plants transfer moisture via transpiration, and therefore latent heat to the atmosphere above. Moisture is drawn from soil by pressure differences within the plants and then transferred to the atmosphere because of the smaller vapor pressure in the atmosphere than in the leaves (or bark), the vapor-pressure deficit (e.g., Monteith, 1965; Oke, 1987, p. 64).

The transfer of moisture from leaves to atmosphere is commonly parameterized by a stomatal resistance, r_s (Monteith, 1965), or its inverse, a stomatal

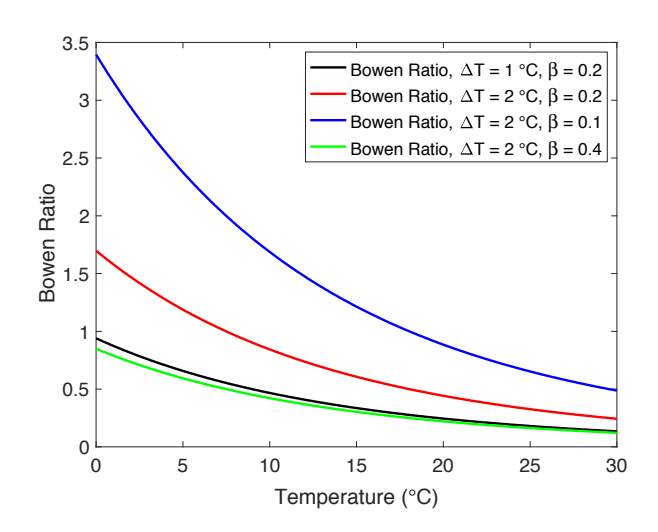


Figure 5. Calculated Bowen ratios, *B*, from Equation 12 as a function of MAT or T_a for different values of ΔT and β with RH = 0.5.

conductance, $g_s = 1/r_s$. By analogy with fluid flow in a pipe, the rate of flow is proportional to the pressure difference, and because specific humidity at saturation, $q^*(T)$, scales with the partial pressure of water vapor, g_s can be expressed with units of speed, in millimeters per second. Values of stomatal conductance or resistance vary with types of vegetation (e.g., grass versus trees), with the extent of leaf cover, and with the degree of saturation of the soil in which the roots grow. The leaf cover is commonly parameterized by the leaf-area index, the dimensionless ratio of the area covered by leaves to that of the surface below; greater leaf cover means lower resistance to vapor transport. Resistance to moisture transfer by an entire forest canopy or grass cover to the air above is then commonly parametrized by a canopy resistance, r_c (or conductance, $g_c = 1/r_c$), that is inversely proportional (or proportional) to the leaf-area index and that increases (or decreases) as soil moisture decreases.

This moisture is then treated as being transferred aerodynamically, or turbulently, to the air further aloft, according to the relationship given by Equation 7 for sensible heat transport (e.g., Betts, 2000). Thus, moisture confronts two resistances treated as in series: a canopy resistance, $r_{\rm c}$, and the aerodynamic resistance, $r_{\rm a} = 1/(c_{\rm T}|v|)$, yielding a combined resistance of $r_{\rm c} + r_{\rm a}$. From Equation 8:

$$\beta = \frac{r_{a}}{r_{a} + r_{c}} = \frac{g_{c}}{g_{a} + g_{c}},$$
(13)

where $g_{\rm a}=c_{\rm T}|{\rm v}|=1/r_{\rm a}$ is the aerodynamic conductance. Over open water, $r_{\rm c}\to 0$, $g_{\rm c}\to \infty$, and $\beta\to 1$; for a completely dry, unvegetated surface, $r_{\rm c}\to \infty$, $g_{\rm c}\to 0$, and $\beta\to 0$.

This treatment of two resistances in series obviously is an oversimplification. As Miralles et al. (2011, 2020) explained, "evapotranspiration" consists of three parts: transpiration; interception, which is the evaporation of precipitation that plants intercept before the liquid water reaches the ground; and evaporation from the underlying soil. Miralles et al. (2011) showed that on a global average and annual basis, evapotranspiration breaks down as 80% transpiration, 11% interception, 7% bare-soil evaporation, and 2% snow sublimation, but as discussed below, such fractions in different regions can differ widely depending on vegetation type. Vegetation resists the transfer of moisture by lengthening the path traversed by moisture that transpires through leaves (and bark) and to a lesser extent by shielding moisture within the soil or on the plants from the atmosphere above the canopy.

As is implied by the dependence of g_a or r_a on wind speed, values of conductance and resistance are not constants. In a particularly detailed study of a boreal spruce forest in Manitoba, Canada, Betts et al. (1999) showed that r_c depends, approximately linearly, on relative humidity of the air, so that at RH \approx 0.25, $r_c \approx 500~(\pm 100)$ s/m and decreases to $r_c \approx 25$ s/m at RH ≈ 0.95 . Resistance is greater when incoming radiation available to the leaves is smaller, and smaller when leaves are wet, such as following rain. They found that although r_c varied little with wind speed, r_a decreased with it, from $r_a \approx 10.5$ s/m at a speed of 2 m/s to $r_a \approx 7$ s/m at 8 m/s, and therefore not inversely with wind speed as suggested by $r_a = 1/(c_T|v|)$ with constant c_T .

Dependence of Surface Conductance or Resistance on Surface Cover

Nature has found ways to balance energy fluxes across surfaces with different land cover, and therefore with different temperature differences between soil and air, ΔT , and with different Bowen ratios, B. Although B scales almost linearly with ΔT , other quantities affect it, and therefore to be a guide to understanding why ΔT differs in regions of different land cover, the effects of these other quantities must be understood. In particular, moisture availability $\beta = r_a/(r_a + r_c)$ depends strongly the nature of the vegetation at the surface (Table 2).

To appreciate how values of SH, LH, B, r_c , and ΔT trade off with one another, it is worth considering the large annual cycles in them. As an example, for a site at high altitude on the Tibetan Plateau, Gu et al. (2005) divided the year into four periods: frozen ground (119 days), pre-growth (72 days), growth (123 days), and post-growth (51 days), with values of SH, LH, B, g_c , and ΔT for each, listed in Table 3. In the frozen period, LH is small, presumably because moisture from the surface is available only through sublimation of ice. Although the surface enthalpy flux (SH + LH) to the atmosphere is not large, most must be transferred as SH, and as expected, the Bowen ratio is large, B = 5.24, and accordingly, $\Delta T = 8.58$ °C is also large. By contrast, >70% of the annual precipitation falls in the growth season, making the ground relatively wet, so LH is large, canopy conductance, q_c , is five times higher than in other seasons, and B = 0.39 is small, though $\Delta T = 5.67$ °C remains guite large. Apparently, much of the precipitation does not evaporate but is temporarily stored in the growing plants and soil. Hao et al. (2007) and Li et al. (2015) gave similarly large ranges of values of B for a semiarid grassland in Inner Mongolia, China, and for a site in southern Tibet, respectively.

Seasonal variations in precipitation over grasslands and savannas also lead to seasonal variations in Bowen ratios. For a subtropical savanna in Burkina Faso, Bagayoko et al. (2007) showed that in wet seasons, canopy conductance, g_c , ranged between 6 and 86 mm/s, but in the dry season it never exceeded 5 mm/s, averaged ~2.6 mm/s, and could be <1 mm/s (corresponding to r_c > 1000 s/m). They also showed that on average $g_a \approx 30 \pm 20$ mm/s, so that β would range from ~0.01 to ~0.5. Accordingly, Bowen ratios range between ~0.2 and 10 with low values in rainy seasons and high values in dry ones. Verhoef (1995) and Verhoef et al. (1999) showed that on a daily basis, Bowen ratios can be as small as 0.1 in wet seasons and as large as 10 in dry seasons.

Regions of water-covered surfaces also illustrate such dependences on annual cycles. Over oceans and lakes with no vegetative resistance to latent heat transfer, $r_{\rm c} \rightarrow 0$ (Oke, 1987, p. 127; Raupach, 1995). Correspondingly from Equations 12 and 13, B commonly is small over oceans and lakes (Table 4) (Oke, 1987, p. 70); ΔT in the numerator and $q^*(T_a)$ in the denominator of Equation 12 govern values of B. The difference between sea-surface temperatures (SSTs) and overlying air temperatures can be several degrees Celsius in winter, but annual averages of them commonly are only ~1 °C (Cayan, 1980) and in the tropics only 0.1 °C (Rubino et al., 2020). It follows that B increases as SSTs decrease. Consistent with these expectations, Hicks and Hess (1977) reported $B \approx 0.07$ for air temperatures over the ocean of 25–28 °C to $B \approx 0.2$

for temperatures of 15–16 °C, and Kondo (1976) reported $B \approx 0.1$ –0.2 for SSTs near 25 °C and $B \approx 0.7$ –0.8 with SSTs near 5 °C.

At the opposite extreme, over deserts where vegetation is sparse, $r_{\rm c}$ is large. This might seem contradictory, for if there were no stomata, how could stomata resist transfer of moisture? Rather, because there are no stomata, they cannot transfer (or conduct) moisture from the subsurface to the overlying air, and resistance is large. Raupach (1995) suggested that $r_{\rm c} \approx 1000$ s/m for deserts, where the aerodynamic resistance $r_{\rm a} \approx 100$ s/m. Hence, $\beta \approx 0.1$, and latent heat flux to the atmosphere should be small, despite commonly high temperatures and corresponding large values of $q^*(T_{\rm a})$ over deserts. As expected, Bowen ratios over deserts tend to be large (Table 4); Oke (1987, p. 70) reported that commonly B > 10.0. Laymon and Quattrochi (2004) reported values of B = 3.4 over dry soil in desert conditions in northeastern Nevada, USA, and values of B = 4.0, 5.3, 12.4, 13.2, and 21.1 depending on the grass, bush, and brush cover. Sturman and McGowan (2009) reported 4 < B < 6, albeit only daily values during the dry season in central Australia.

With relatively small latent heat to the atmosphere over desert regions, sensible heat cannot be small, and therefore ΔT tends to be large. In one focused study on the desert of western Utah, USA, Bartlett et al. (2006) measured $\Delta T = 2.47$ °C, larger than most measurements elsewhere. The observations by Burgener et al. (2018), Gallagher et al. (2019), Lu et al. (2019), and others reported above that large values of ΔT in warm seasons tend to occur where rainfall is low also accord with large values of ΔT in deserts. For example, the largest value of ΔT for "bacterial growth seasons" (March–November) that Lu et al. (2019, their figure 2) reported is $\Delta T \approx 6$ °C, but they reported $\Delta T > 9$ °C in summer in that desert (Lu et al., 2019, their supplementary figure 3).

For vegetated regions, Oke (1987, p. 70) stated that "Typical average values of [*B*] are...0.1 to 0.3 for tropical wet jungles; 0.4 to 0.8 for temperate forests and grassland; 2.0 to 6.0 for semiarid areas." A compilation from subsequent published literature yields similar ranges (Table 4).

For grasslands and savannas, where most vegetation is close to the ground and the surface is smooth, we might expect canopy resistance, r_c , to be smaller than over deserts, but greater than that over dense forest canopies with long paths from soil to leaves. Oke (1987, p. 127) gave values of r_a = 70 s/m and r_c = 70 s/m over short grass, and hence β = 0.5. Accordingly, Bowen ratios over such regions are greater than those of open water but less than those over more arid sites (Table 4).

At the opposite extreme, for wetlands with free-standing water near the surface, the availability of moisture facilitates the transfer of latent heat so that canopy resistance, r_c , tends to be small, β tends not to be small, and Bowen ratios, B, are accordingly small (Oke, 1987, p. 70). Moreover, we might expect B to be smaller where regions are hot, as in the tropics, than in temperate wetlands because in hot, moist regions, $q^*(T_a)$ is especially large, and therefore B is small (Fig. 5). For a wet tropical forest in the Amazon region, da Rocha et al. (2004) reported values of conductance of $g_a = 28.7 \pm 7.3$ mm/s and $g_c = 12.7 \pm 4.4$ mm/s, corresponding to $\beta = 0.31 \pm 0.04$, and they reported a relatively small $B = 0.17 \pm 0.10$. By comparison, in a boreal wetland site, den Hartog et

TABLE 2. AERODYNAMIC AND VEGETATIVE CONDUCTANCE AND RESISTANCE OVER DIFFERENT LAND-SURFACE COVER TYPES

Environment	$g_{\rm a}$ (mm/s)	$g_{ m c}$ (mm/s)	β	Reference
Conductance				
Semiarid steppe, Inner Mongolia*	_	4.19	_	Chen et al. (2009)
Semiarid steppe, Inner Mongolia*	_	2.54	_	Chen et al. (2009)
Semiarid steppe, Inner Mongolia*	_	2.46	_	Chen et al. (2009)
Arid steppe, Mongolia	_	2.4	_	Li et al. (2006)
Tropical forest, Amazonia	29 ± 7	13 ± 4	0.31 ± 0.04	da Rocha et al. (2004)
Tropical forest, eastern Amazon	143	13	0.08	Sommer et al. (2002)
Tropical palm forest, Vanuatu	_	2.5–18	_	Roupsard et al. (2006)
Wet temperate grassland, Japan	15	12	0.44	Li et al. (2005)
Wet grassland (in general)	25	60	0.29	Betts (2000)
Temperate alpine meadow, Tibet	_	5	_	Gu et al. (2005)
Temperate grassland, California, USA	_	4	_	Ryu et al. (2008)
Subtropical pine forest, southeastern China	_	11	_	Tang et al. (2014)
Semiarid grasslands, Arizona, USA [†]	8.8	2.6	0.23	Krishnan et al. (2012)
Semiarid grasslands, Arizona, USA [†]	9.2	1.9	0.17	Krishnan et al. (2012)
Boreal forest (in general)	25	900	0.03	Betts (2000)
Boreal black spruce forest [†] *	_	5–10	—	Arain et al. (2003)
High alpine steppe, central Tibet*	_	3.5	_	Ma et al. (2015)
Sub-alpine steppe, central ribet Sub-alpine spruce forest, northeastern Tibet*	350	3	0.009	Zhu et al. (2014)
				. ,
Environment	r _a (s/m)	<i>r</i> _c (s/m)	β	Reference
Resistance				
Open water (in general)	100	0.0	1.0	Chen et al. (2009)
Lakes (in general)	240	0.1	1.0	Raupach (1995)
Semiarid grassland	33 ± 2	340 ± 70	0.09	Yue et al. (2018)
Short grass, pasture (in general)	70	70	0.5	Oke (1987, p. 127)
Meadow (long grass)	20	50	0.3	Monteith (1965)
Grasslands (in general)†*	35	244	0.13	Wilson et al. (2002)
Annual grassland	75	10–3000	0.5§	Baldocchi and Ma (2013)
Prairie	20–30	20–150	0.12-0.5	Monteith (1965)
Mediterranean climates (in general)†*	21	654	0.031	Wilson et al. (2002)
Wooded savanna	25	70–1000	0.051 0.25§	Baldocchi and Ma (2013)
Pine forest	6	90	0.06	Monteith (1965)
Boreal black spruce forest, late summer	20			Baldocchi and Vogel (1996
Temperate broad-leaved forest, late summer	5	_	_	Baldocchi and Vogel (1996
Forests (in general)	20	200	0.09	Raupach (1995)
` ` ` ,	5–10	80–150		. ,
Forests (in general) Coniferous forests (in general) [†] *	5–10 16	120	0.03–0.13 0.12	Oke (1987, p. 127)
` • · · · · · · · · · · · · · · · · · ·	20	120 72		Wilson et al. (2002)
Deciduous forests (in general) [†] * Boreal tundra [†] *	20 43	72 175	0.22 0.20	Wilson et al. (2002)
- Control of the Cont				Beringer et al. (2005)
Boreal low shrub [†] *	21 24	170	0.11	Beringer et al. (2005)
Boreal wasdland [†] *		172	0.12	Beringer et al. (2005)
Boreal woodland [†] *	13	146	0.08	Beringer et al. (2005)
Boreal forest ^{†*}	11	169	0.06	Beringer et al. (2005)
Deserts (in general)	108	2000	0.05	Raupach (1995)

Note: As discussed in the text section "Moisture Availability, β, and Resistance to (or Conductance of) Moisture by Different Land-Surface Cover, g_a is aerodynamic conductance, g_c is vegetative conductance, r_a is aerodynamic resistance, r_c is vegetative resistance, and β is moisture availability. See text Equation 8. Dash indicates data not available.

^{*}Midday.

[†]Growing season. §Annual average values estimated using values when latent heat flux is large.

TABLE 3. SURFACE FLUXES AND RELEVANT PARAMETERS FOR A SITE ON THE TIBETAN PLATEAU*

Season	Frozen	Pre-growth	Growth	Post-growth	Annual†
Duration (days)	119	72	123	51	365
Precipitation (mm)	11.6	121.8	394.7	14.7	542.8
Sensible heat flux, SH (MJ/m²/day)	1.9	2.8	2.0	3.5	2.33
Latent heat flux, LH (MJ/m ² /day)	0.4	1.3	5.2	1.4	2.33
Bowen ratio, B	5.24	2.09	0.39	2.61	1.00
Air temperature, Ta (°C)	-12.08	0.06	9.12	-1.38	-1.05
Soil temperature, T _s (°C)	-3.50	-3.94	14.79	4.69	5.28
$\Delta T = T_s - T_a$ (°C)	8.58	2.88	5.67	6.07	6.33
Canopy conductance, $g_{\rm c}$ (mm/s)	2.07	2.17	11.0	2.54	4.80

^{*}From Gu et al. (2005).

al. (1994) reported a range from $B \approx 1.5$ when surface temperatures were only 10–15 °C dropping to $B \approx 0.8$ when surface temperatures rose 25 °C, consistent with the increase in $q^*(T_a)$ as T_a rises.

The most complicated and diverse environments are forests, for which values of r_c or q_c , β , and B tend to lie intermediate between those of wetlands and savannas or grasslands. Raupach (1995) gave $r_c = 200$ s/m for forests, compared with 1000 s/m for deserts, whose surfaces can be rough, and 0.1 s/m for lakes, whose surfaces are relatively smooth. Although one might expect stomatal resistances to differ for different species of trees, including the difference between angiosperms with leaves and gymnosperms with needles, such differences seem to be small compared with differences in average canopy cover (e.g., Kelliher et al., 1995). By considering "'maximum' stomatal and surface conductance, those which describe the stomatal properties of a vegetated surface with plentiful soil water, adequate light, low humidity deficit and optimal temperature," Kelliher et al. (1995, p. 3) inferred nearly indistinguishable maximum values of stomatal conductance of grasslands of 17.0 ± 2.1 mm/s and of forests of different types of 19.7 ± 1.5 mm/s, though Kelliher et al. (1998) did report values of g_c less than half as large for boreal pine forests. A dense canopy shields the surface from the atmosphere more than an open canopy. As important as the leaf-area index, however, are the amount of soil moisture available to trees and the specific humidity of the air into which the moisture is transferred (e.g., Baldocchi et al., 1997). The latter two quantities define the vapor-pressure deficit between air and leaf, which scales with canopy conductance (e.g., Oke, 1987; Raupach, 1995; Wallace, 1995).

Forests with a canopy well above the surface shield both that surface and moist vegetation below the canopy from relatively high winds above it, and canopy resistance, r_c , varies markedly with both soil moisture and liquid water on leaves (e.g., Wallace, 1995). Wang et al. (2009) reported that for three different boreal forests in Canada, the ratio of latent heat extracted from the soil to the total latent heat flux transferred to the atmosphere above the canopy ranged from as little a 0.05 for Southern Old Aspen to 0.14 for the Southern Old Black Spruce and to 0.34 for the Southern Old Jack Pine. Vegetation below

the canopy can also be a direct source of moisture to the atmosphere above the canopy, ranging from 25% of the total for a boreal aspen forest (Blanken et al., 1997) to 20%–40% for a boreal jack pine forest (Baldocchi et al., 1997) to 54% for a boreal *Pinus sylvestris* forest in Siberia (Kelliher et al., 1998). In this respect, there is a suggestion that although the stomatal resistances of angiosperms (e.g., aspen) and gymnosperms (e.g., pine) are similar (Kelliher et al., 1995), the total canopy resistance, from surface to free air above, is greater for aspen than for pine (Kelliher et al., 1998).

With tall trees, stomatal resistance tends to be larger than that of short grasses (e.g., Stewart and Thom, 1973), but conversely, the rough surface of the canopy leads to smaller aerodynamic resistance than over the smoother grass surface. Transfer of moisture from below a canopy to above it requires turbulent transfer that is scaled by an aerodynamic resistance, whose value presumably is not the same as that parameterized by r_a. The latter takes into account the moisture transferred from the upper story to the atmosphere above, where winds are different from those extracting moisture from the soil. Because the aerodynamic resistance, r_a , varies inversely with wind speed, choosing an appropriate value for r_a is hardly straightforward, given the differences in wind speeds above and below the canopy. Moreover, winds near the floor vary with forest type; Baldocchi et al. (2000) reported more concentrated winds near the floor of a boreal jack pine forest than beneath a ponderosa pine forest with more widely spaced trees. Because the enthalpy flux coefficient, c_{T} , is greater for rough than smooth surfaces, the irregular surface created by the canopy leads to a relatively large value of c_T and therefore a small value of r_a . McColl (2020) used forests to exemplify the "rough limit," where a rough surface enhances turbulence, so that g_a becomes large and r_a becomes small.

Clearly, one size of either r_a or r_c does not fit all forests. The combination of processes that bring moisture to the overlying air above forests and therefore that enhance latent heat transfer, and the weak winds at the surface, which affect sensible heat transfer, lead to small Bowen ratios and small values of ΔT . For example, $\Delta T = 0.6 \pm 0.6$ °C for a boreal Scots pine forest in Finland (Launiainen, 2010).

A Contrast Illustrating Differences in ΔT for Different Resistances of Surface Cover

A pair of sites in central California, USA, only 2 km apart, one a wooded oak savanna with ~40% cover by trees (Tonzi Ranch) and the other a grassland (Vaira Ranch), offers a useful contrast (e.g., Baldocchi et al., 2004). The greater albedo of the grassland makes incident shortwave energy over the oak savanna the greater; ignoring uncertainties, the mean annual radiation to the oak savanna, $104.4 \pm 8.8 \, \text{W/m}^2$, exceeds that to the grassland $92.7 \pm 18.4 \, \text{W/m}^2$ (Baldocchi and Ma, 2013). The air temperature over the savanna, however, is only slightly, and insignificantly, greater, by $0.56 \pm 0.71 \, ^{\circ}\text{C}$, than that over the grassland (Baldocchi and Ma, 2013), and hence differences in longwave energy radiated from the surfaces must be small. Both latent and sensible heat fluxes to the overlying air

[†]Calculated using seasonal values weighted by their durations.

TABLE 4. VALUES OF BOWEN RATIOS IN DIFFERENT SETTINGS

Environment	Place	Bowen ratio	Reference
Subtropical ocean	Near San Diego, California, USA	0.1	Pond et al. (1971)
Subtropical ocean	Near Barbados	0.1	Pond et al. (1971)
Subtropical ocean	Gulf of Mexico	0.1	Hsu (1998)
Subtropical ocean	East China Sea	0.1	Kondo (1976)
Subtropical ocean	Indian Ocean	≤0.1	Rao et al. (1986)
Subtropical ocean	East China Sea	0.07-0.2	Hicks and Hess (1977)
Mid-latitude ocean	East China Sea	0.8	Kondo (1976)
Tropical forest	Amazon Basin	0.17 ± 0.10	da Rocha et al. (2004)
Tropical forest	Amazon Basin	0.35	von Randow et al. (2004)
Tropical palm plantation	Vanuatu	0.39 (0.16-0.59)	Roupsard et al. (2006)
Subtropical pine forest	China	0.35 ± 0.06	Tang et al. (2014)
Wet temperate grassland	Japan	0.2	Li et al. (2005)
Deciduous forests*	Northern Hemisphere	0.42	Wilson et al. (2002)
Deciduous forests	Northern Hemisphere	0.3-1.5	Eugster et al. (2000)
Conifer forests*	Northern Hemisphere	1.07	Wilson et al. (2002)
Temperate Douglas-fir forest	British Columbia, Canada	0.55	Humphreys et al. (2003)
Temperate deciduous forest	Indiana, USA	0.59 ± 0.02	Oliphant et al. (2004)
Temperate spruce forest	Germany	0.69 ± 0.19	Grünwald and Bernhofer (2007)
Temperate deciduous forest	Tennessee, USA	0.72	Wilson and Baldocchi (2000)
Temperate pine plantation	North Carolina, USA	0.89 ± 0.7	Sun et al. (2010)
Temperate mixed forest	China	0.74	Wu et al. (2007)
Temperate Alpine meadow	China	1.0	Gu et al. (2005)
Temperate steppe	China	1.2	Hao et al. (2007)
Temperate grassland	California, USA	1.9	Ryu et al. (2008)
Boreal Wetlands	Northern Ontario, Canada	1.03-1.11	den Hartog et al. (1994)
Arctic and Boreal Wetlands	Northern Hemisphere	0.2-0.7	Eugster et al. (2000)
Low Arctic shrub tundra	Northern Hemisphere	0.3–1.5	Eugster et al. (2000)
Boreal shrub	Northern Hemisphere	0.5-1.0	Eugster et al. (2000)
Low Arctic upland tundra	Northern Hemisphere	0.4–1.0	Eugster et al. (2000)
Forest tundra	Northern Hemisphere	0.4–1.7	Eugster et al. (2000)
Dark taiga (spruce and fir)	Northern Hemisphere	0.7–1.5	Eugster et al. (2000)
Low Arctic coastal tundra	Northern Hemisphere	0.6–2.1	Eugster et al. (2000)
High Arctic coastal tundra	Northern Hemisphere	0.8–2.5	Eugster et al. (2000)
Light taiga (pine and larch)	Northern Hemisphere	0.6–3.8	Eugster et al. (2000)
Boreal Scots pine forest	Finland	0.81 ± 0.27	Launiainen (2010)
Sub-Alpine Spruce forest	China	2.2	Zhu et al. (2014)
Alpine steppe	Tibet	1.95	Ma et al. (2015)
Mediterranean climates*	Northern Hemisphere	17.9	Wilson et al. (2002)
Open woodland and savanna	South Africa	1.5 ± 1.0	Majozi et al. (2017)
Shrub and grasslands [†]	Utah, USA	0.4	Malek et al. (1990)
Grasslands*	Northern Hemisphere	0.89	Wilson et al. (2002)
Desert, playa [†]	Utah, USA	2.45	Malek et al. (1990)
Semiarid grassland	China	1.3 ± 0.3	Yue et al. (2018)
Arid steppe	Mongolia	2.2	Li et al. (2006)
Desert [†]	Australia	4.08	Sturman and McGowan (2009)
Desert [†]	Australia	4.46	Sturman and McGowan (2009)
Desert [†]	Australia	5.38	Sturman and McGowan (2009)
Desert [†]	Australia	5.63	Sturman and McGowan (2009)
Desert [†]	Australia	6.12	Sturman and McGowan (2009)
Desert	Nevada, USA	3.43	Laymon and Quattrochi (2004)
Desert	Nevada, USA	4.04	Laymon and Quattrochi (2004)
Desert	Nevada, USA Nevada, USA	12.43	Laymon and Quattrochi (2004)
Desert	Nevada, USA Nevada, USA	21.1	Laymon and Quattrochi (2004)
Desert			Laymon and Quattrochi (2004)
	Nevada, USA	13.21 5.26	
Desert	Nevada, USA	5.20	Laymon and Quattrochi (2004)

^{*}Warm season only.
†Dry season only.

above the wooded savanna are greater than those from the grassland, but Bowen ratios are similar for them, although published values differ: for the wooded savanna, B = 1.58 (Baldocchi and Ma, 2013), $B = 1.95 \pm 0.35$ (Baldocchi et al., 2010), and $B = 1.92 \pm 0.35$ (this study); and for the grassland, B = 1.86 (Baldocchi and Ma, 2013) and $B = 2.04 \pm 0.34$ (this study). The much deeper roots of the trees in the wooded savanna draw moisture from below the soil sampled by the grass and sustain latent heat transfer in summer when the grass not only dries out, but also by becoming "golden," increases its albedo relative to that when it is green (Baldocchi and Xu, 2007; Baldocchi et al., 2004, 2021; Ma et al., 2016).

The relatively small differences in the various energy fluxes belie a large difference between soil and air temperatures: for the wooded savanna, $\Delta T =$ 1.25 ± 0.40 °C, but for the grassland, $\Delta T = 3.08 \pm 0.77$ °C. Let us treat the Bowen ratios as essentially equal, and in the definition of B in Equation 12, let us consider the factor $\Delta T/(1 + 0.07\Delta T - RH)$. With RH = 0.6, this factor is 2.56 for the wooded savanna and 5.00 for the grassland. This suggests that the value of $\beta_{gr} = r_a/(r_a + r_c)$ for the grassland, given by Equation 13 and in the denominator of B in Equation 12, should be about two times greater than that for the wooded savanna, β_{ws} : $\beta_{gr} \approx 2\beta_{ws}$. Values of aerodynamic resistance, r_a , over the two areas indeed differ by a factor of two throughout the year, varying between summer and winter between ~50 and 100 s/m for the grassland and between 25 and 50 s/m for the wooded savanna (Baldocchi and Ma, 2013). The greater roughness of the forest than the grass accounts for the differences in aerodynamic resistance. Values of canopy resistance to water vapor, r_c, range over larger values from 10 to ~3000 over the grassland and 70 to 1000 over the savanna, but in the moist season when latent heat is greatest, between Julian days 50 and 150, they are roughly equal. Thus, to a first approximation, differences in moisture availability, β, associated with different aerodynamic resistances, r_a , can account for the difference between values of ΔT .

■ MEASURED DIFFERENCES BETWEEN T_s AND T_a FOR DIFFERENT TYPES OF LAND COVER

As noted above, the FLUXNET2015 data set provides a wealth of data on surface enthalpy fluxes, SH and LH, and temperatures, $T_{\rm s}$ and $T_{\rm a}$. To avoid inclusion of possibly aberrant years, among the data available from the FLUXNET2015 data set, I used only sites with at least two complete years of data (156 sites). Although the FLUXNET2015 database includes data from 10 IGBP surface-cover categories (Table 1), similarities of some of these allow them to be lumped into five categories: (1) permanent wetlands, (2) forests of differing compositions, (3) closed and open shrublands, (4) savannas and woody savannas, and (5) grasslands. Unfortunately, there are no sites from deserts. See data provided in the Supplemental Material 1.

Confining analysis of data in the FLUXNET2015 data set to annual average values of SH, LH, $T_{\rm s}$, and $T_{\rm a}$ may be a risk because, as discussed above, many geologic measures of soil temperatures might not be sensitive to conditions when temperatures are below freezing. Given that processes that record soil temperatures slow, if not cease completely, when the ground is frozen, the discussion below separates sites whose mean annual temperatures (MATs) are $\Delta T \lesssim 5$ °C from those with warmer mean annual conditions.

Permanent Wetlands

Sixteen (16) sites assigned to permanent wetlands with data for two years or more include six at latitudes >60° and hence from relatively cold regions. Among the 16 sites, 13 reported both $T_{\rm s}$ and $T_{\rm a}$. For cold regions, with MAT < 0 °C, values of ΔT can be large, with $\Delta T > 3.5$ °C for six of them and $\Delta T > 7$ °C for two (Fig. 6A). For the five sites with MAT \gtrsim 5 °C, however, $\Delta T \lesssim$ 2 °C. Despite these sites being designated as wetlands, when MAT < 0 °C, low $T_{\rm s}$ leads to small values both of heat radiated from the surface, $Q_{\rm LW}$ (proportional to $T_{\rm s}^4$), and of latent heat flux, LH, proportional to specific humidity, $q^*(T_{\rm a})$. Thus, the numerator in Equation 11 is relatively large, and a large fraction of the enthalpy flux from the surface must be transferred as sensible heat flux. Accordingly, ΔT must be relatively large, as observed (Fig. 6A).

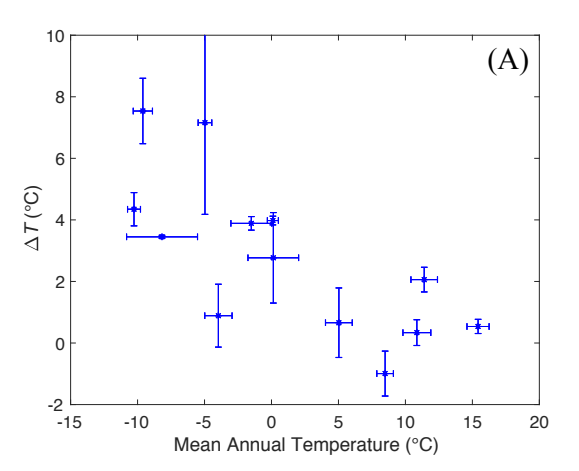
For all 16 sites, Bowen ratios $B \lesssim 1$, and for most of these, $B \lesssim 0.5$, and the mean is 0.37 ± 0.48 (Fig. 6B). This might seem inconsistent with the relatively large values of ΔT . The availability of moisture in summer (large β) at such sites, particularly those at high latitudes where energy fluxes are small, surely contributes to small values of Bowen ratios. For the eight stations where MAT > 5 °C, Bowen ratios decrease with increasing MAT, if a bit more steeply than if proportional to $q^*(T_a)$; the red line in Figure 6B shows how values of B would decrease with temperature if its dependence on $T_a = MAT$ scaled with $q^*(T_a)$ in Equation 12, such that at MAT = 0 °C, B = 1.0, and with identical values of other parameters (ΔT , β , RH, and surface air pressure). Thus, values of B and ΔT are consistent with the theoretical arguments given above. Although data are few, they suggest that for MAT < 0 °C, ≈ 4 –6 °C, but for MAT > 5 °C, $\Delta T \lesssim 2$ °C.

Forested Regions

The FLUXNET2015 data set includes 85 sites designated as forested (omitting one that was affected by recent fires) and with at least two years of data. Among the five forested land-cover designations by the IGBP (Table 1), the FLUXNET2015 database includes evergreen needleleaf, evergreen broadleaf, deciduous broadleaf, and mixed forests, but no sites with sufficient data from a fifth forest category, deciduous needleleaf forests. Among these 85 stations, the FLUXNET2015 data set reported values of ΔT from 77 of them.

As is the case for permanent wetlands, the largest values of ΔT are found where regions are especially cold (Fig. 7A), with many values of $\Delta T > 3$ °C.

¹Supplemental Material. The complete data used in text Figures 7–11. Please visit https://doi.org/10.1130/GEOS.S.16850659 to access the supplemental material, and contact editing@geosociety.org with any questions.



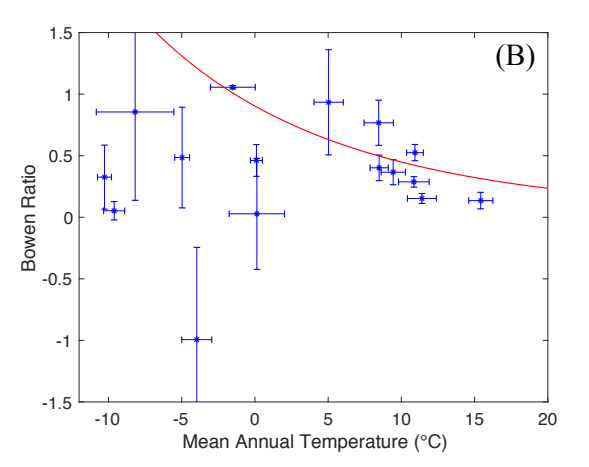


Figure 6. Results from the FLUXNET2015 database for permanent wetlands. Error bars show standard deviations. (A) Values of ΔT , the difference between soil temperature, T_s , and that of the overlying air, Ta, versus mean annual temperatures, MAT. (B) Values of the Bowen ratio, B. versus MAT. The red line shows values of the Bowen ratio calculated assuming that it depended only on the saturation specific humidity of the air at temperature T_a , $q*(T_a)$, in the denominator of Equation 12 such that $T_a = MAT$ and B= 1.0 at MAT = 0 °C. It is not a fit to data, but merely a curve showing the effect of $q^*(T_a)$ on B.

Again, cold air leads not only to low values of longwave radiation from the surface, Q_{LW} , but also to small latent heat flux, LH, and therefore to large values in the numerator of Equation 11 and relatively large observed values of ΔT .

If we confine ourselves to sites with MAT $\gtrsim 5$ °C, only for a few is $\Delta T > 2$ °C, and for only one (site ZM-Mon from Zambia in the tropics, with only three years of data) does ΔT exceed 2 °C by more than its standard deviation (Fig. 7A). Moreover, the majority are indistinguishable from $\Delta T = 0$ °C. The mean value of ΔT for the 59 sites with MAT ≥ 5 °C is -0.90 ± 0.62 °C. As discussed above, the conductance of moisture from the canopy, g_c , can be greater than the aerodynamic conductance, g_a , which makes moisture availability, β , given by Equation 13, relatively large. Consistent with values of ΔT decreasing with increasing MAT, Bowen ratios also decrease with increasing MAT (Fig. 7B), from B > 2 for MAT < 0 °C to B < 0.5 for MAT $\gtrsim 15$ °C. The red line in Figure 7B shows how B would vary with MAT if that temperature were the only parameter affecting B.

If mean annual precipitation is used as a surrogate for aridity, and restricting sites to those with MAT \geq 5 °C, the relatively large values of both ΔT (Fig. 7C) and Bowen ratios (Fig. 7D) come from regions where mean annual precipitation is not great, <1200 mm. The decrease in Bowen ratios with mean annual precipitation (Fig. 7D) shows a clearer pattern than that for ΔT , but again this decrease concurs with the greater role of sensible heat transfer in arid than in humid regions.

The data from forested regions in Figure 7 suggest that where MAT \gtrsim 5 °C, $\Delta T \lesssim$ 2 °C, but in colder regions, ΔT can exceed 2 °C.

Shrublands, Open and Closed

Although data are fewer than from forests, values of ΔT from shrubland sites share similarities with those of forests and wetlands. For MAT \lesssim 0 °C, ΔT > 3 °C and is largest, ΔT = 6.5 \pm 0.5 °C, for the lowest MAT (Fig. 8A), presumably

again because sensible heat flux should be more important than latent heat flux where MATs are low. For three among the seven sites with MAT > 5 °C, however, ΔT is quite large: ΔT > 3 °C (Fig. 8A). The processes controlling energy balance over the regions with low and high MAT should be different, and Bowen ratios offer some insight into these differences. Values of B for MAT \lesssim 0 °C (Fig. 8B) are comparable to those for forests (Fig. 7B), suggesting that the large values of ΔT in the numerator of Equation 12 are offset by the small values of $q^*(T_a)$, as observed for forests. With much scatter and unlike for forests (Fig. 7B), however, B tends to increase with ΔT (Fig. 8B).

Regardless of whether only sites with MAT > 5 °C or all sites are used, ΔT decreases with mean annual precipitation (Fig. 8C). This trend is consistent with ΔT increasing with increasing aridity, for which latent heat fluxes become small. As with wetlands and forests (Fig. 7D), and consistent with this logic, the largest Bowen ratios are found where mean annual precipitation is small, <500 mm (Fig. 8D).

Results from only two sites characterized by closed shrubland, and therefore with more vegetative cover than where shrublands are open, cannot define a pattern. Nevertheless, the small values of ΔT (Figs. 8A and 8C) are consistent with smaller aerodynamic resistance and correspondingly smaller Bowen ratios than where shrublands are open, and with *B* decreasing with mean annual precipitation (Figs. 8B and 8D).

Savannas and Woody Savannas

The 12 savanna and four woody savanna sites lie in warm climates, with MAT > 15 °C (Fig. 9A). For most, ΔT > 3 °C, and the mean of the 16 values of ΔT is 3.8 ± 1.2 °C. There is little variation in ΔT with precipitation (Fig. 9C), and if two relatively small values of ΔT for woody savannas are ignored, $\Delta T \approx 4$

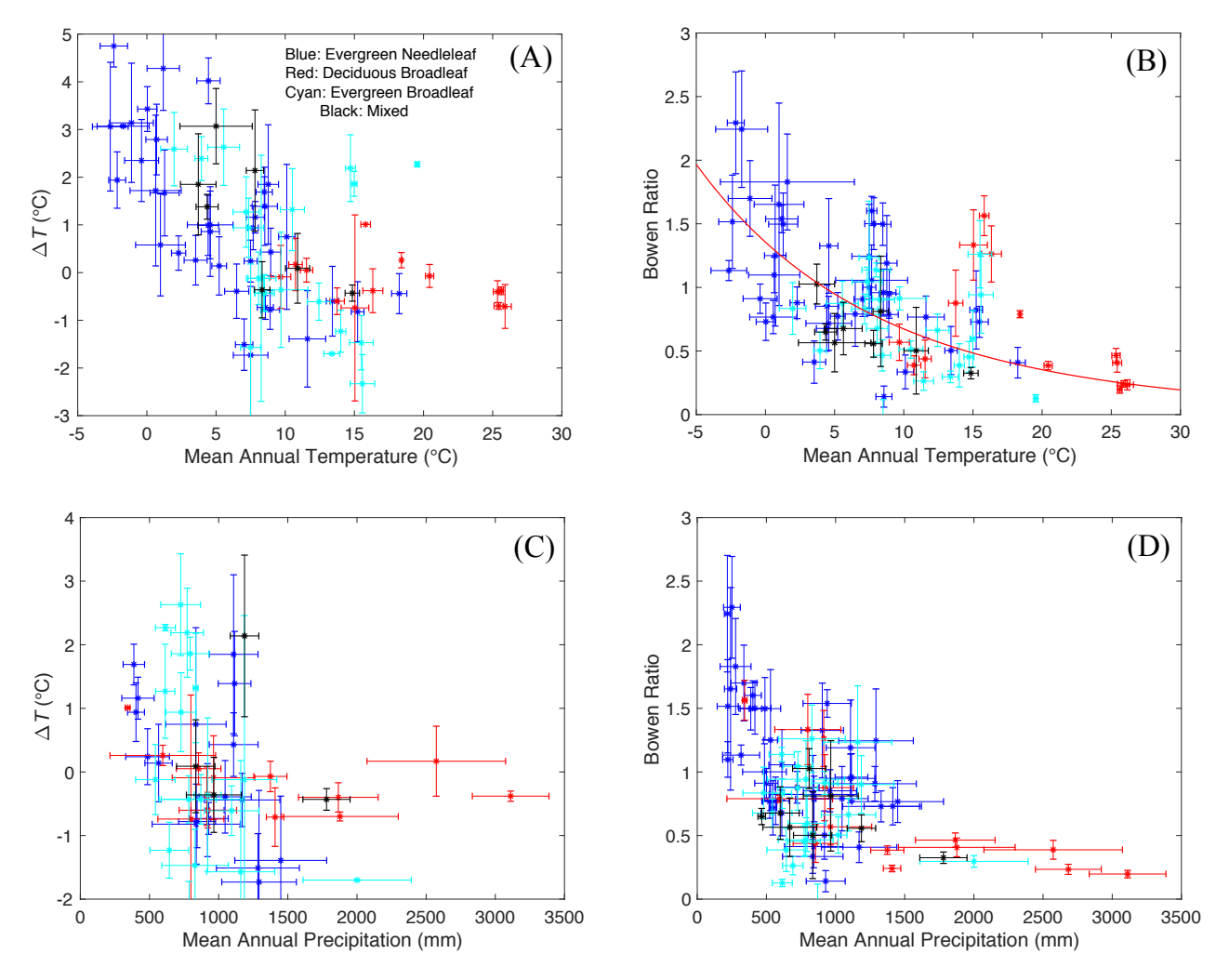


Figure 7. Results from the FLUXNET2015 database for forests of different kinds. (A) Values of ΔT , the difference between soil temperature, T_s , and that of the overlying air, T_a , versus mean annual temperatures, MAT. (B) Values of the Bowen ratio, B, versus MAT. The red line shows values of the Bowen ratio calculated assuming that it depended only on the saturation specific humidity of the air at temperature T_a , $q^*(T_a)$, in the denominator of Equation 12, such that $T_a = \text{MAT}$ and B = 1.5 at MAT = 0 °C. As with Figure 6B, this is not a fit to data, but a curve that illustrates the dependence of B on $T_a = \text{MAT}$ via $q^*(T_a)$. (C) Values of ΔT versus mean annual precipitation, a surrogate for aridity, for stations with MAT ≥ 5 °C. (D) Values of the Bowen ratio, B, versus mean annual precipitation for stations with MAT ≥ 5 °C.

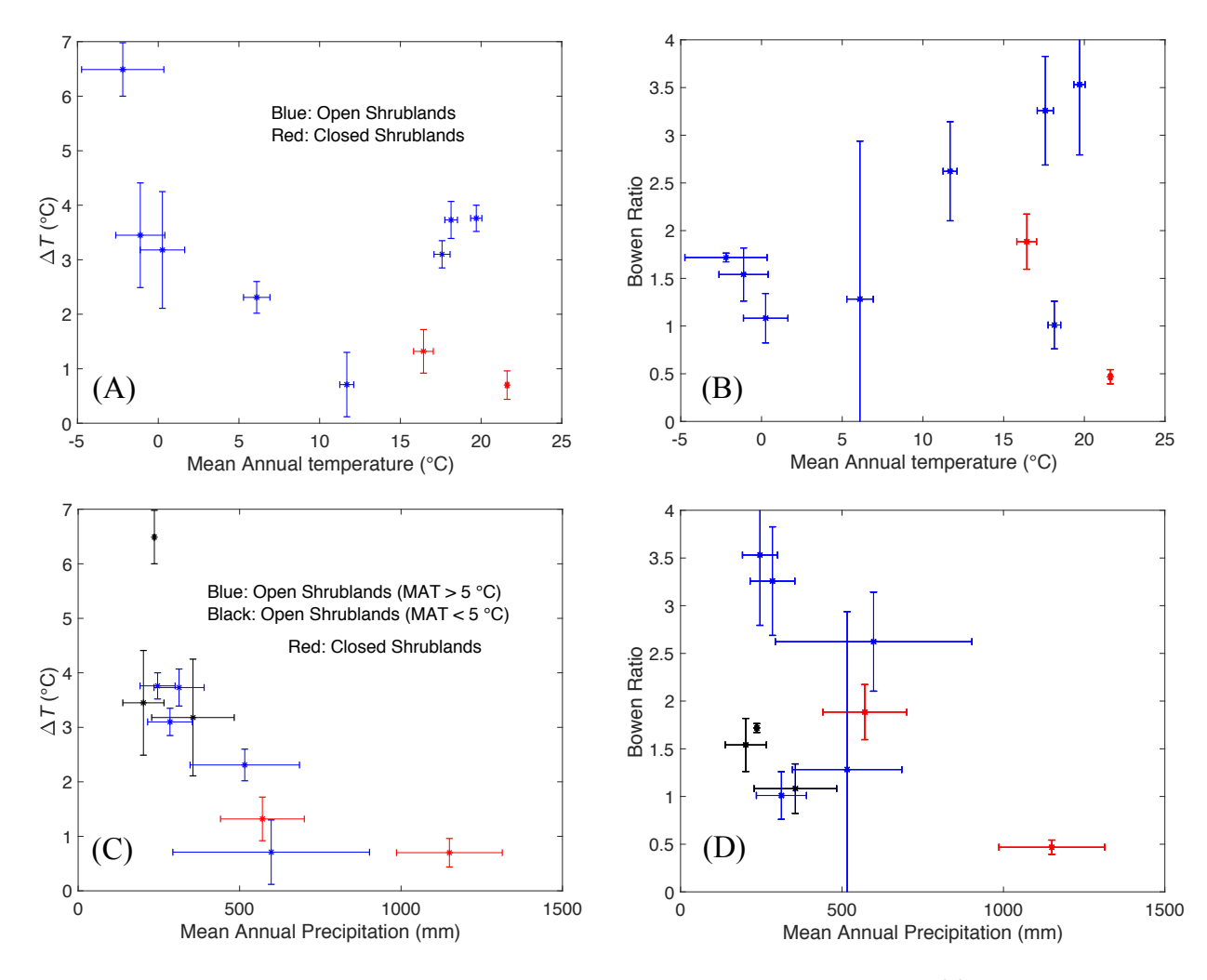


Figure 8. Results from the FLUXNET2015 database for closed and open shrublands. Error bars show standard deviations. (A) Values of ΔT , the difference between soil temperature, T_s , and that of the overlying air, T_a , versus mean annual temperatures, MAT. (B) Values of the Bowen ratio, B, versus MAT. (C) Values of ΔT versus mean annual precipitation, a surrogate for aridity. (D) Values of the Bowen ratio versus mean annual precipitation.

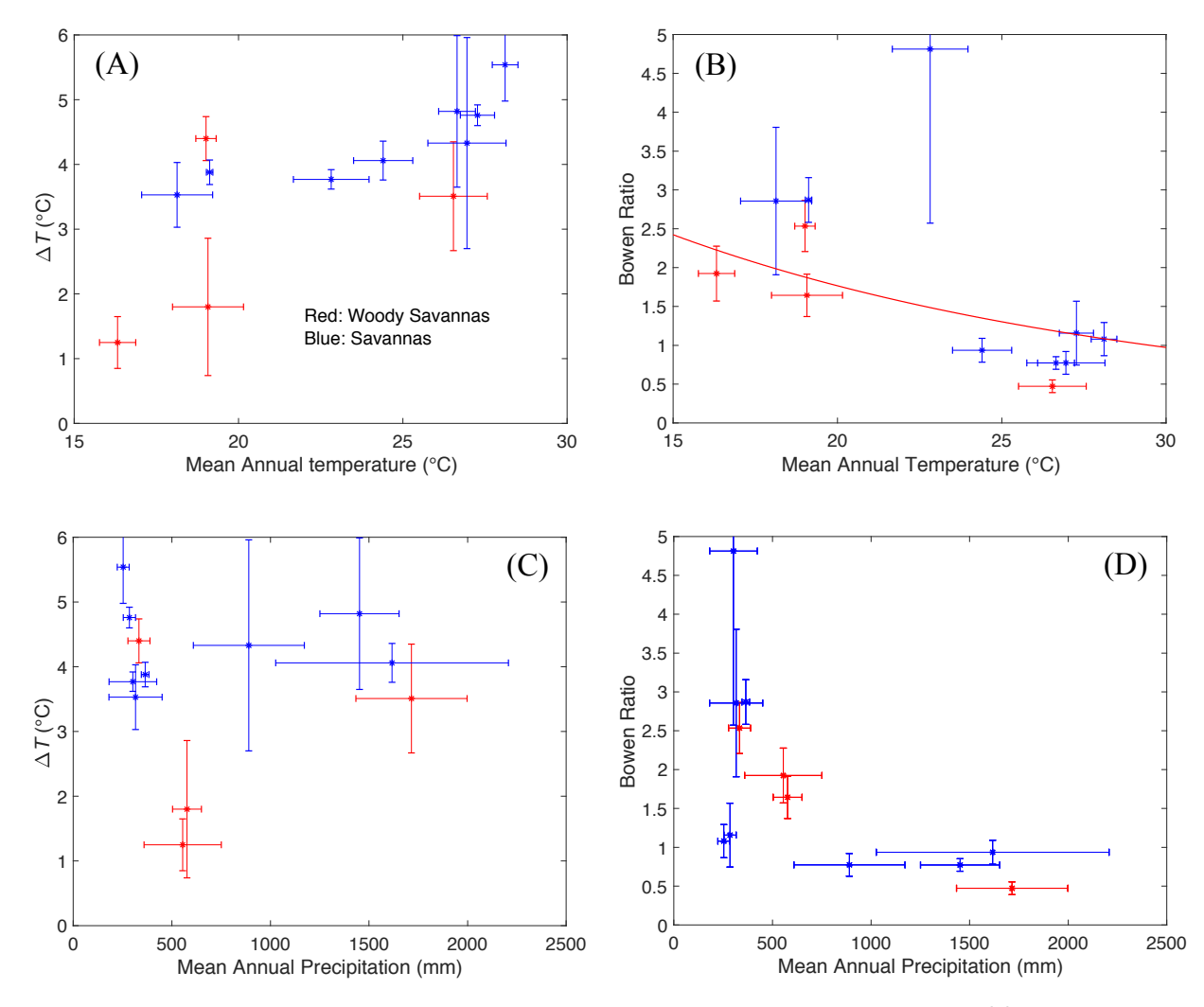


Figure 9. Results from the FLUXNET2015 database for savannas and woody savannas. Error bars show standard deviations. (A) Values of ΔT , the difference between soil temperature, $T_{\rm s}$, and that of the overlying air, $T_{\rm a}$, versus mean annual temperatures, MAT. (B) Values of the Bowen ratio, B, versus MAT. The red line shows values of the Bowen ratio calculated assuming that it depended only on the saturation specific humidity of the air at temperature $T_{\rm a}$, $q^*(T_{\rm a})$, in the denominator of Equation 12 such that $T_{\rm a} = {\rm MAT}$ and $T_{\rm a} = {\rm MAT}$

 \pm 1 °C. Alternatively, including those two values, ΔT increases roughly linearly with MAT (Fig. 9A). Climates in the exceptional regions where $\Delta T < 2$ °C—the Tonzi Ranch in the Sierran foothills of California, discussed above, and site FLX-AU-Gin just north of Perth, western Australia—are characterized by Mediterranean climates where precipitation occurs in winter, and summers are hot and dry. Thus, wet seasons are out of phase with those with large radiative fluxes, and this might make these sites different from those in other settings.

For warm regions, where $q^*(T_a)$ increases markedly with temperature, we might expect Bowen ratios to decrease with increasing temperature. The decrease in B with MAT is, at best, crudely consistent with this expected dependence of q^* on MAT (Fig. 9B), though the increase in ΔT with MAT surely contributes to the scatter. Because moisture availability, β , depends on soil moisture, which should decrease with precipitation, an inverse dependence of B on precipitation seems likely and adequately describes the pattern except for two sites with relatively small values of B (< 1.5) and low mean annual precipitation (300 mm) (Fig. 9D).

Grasslands

Thirty-one (31) grassland sites in the FLUXNET2015 database include a wide range of values of both MAT and ΔT . The assignment of "grassland," however, appears to be somewhat misleading, because for all, the standard description (e.g., http://sites.fluxdata.org/AT-Neu/) includes: "Grasslands: Lands with herbaceous types of cover. Tree and shrub cover is less than 10%. Permanent wetlands lands (sic) with a permanent mixture of water and herbaceous or woody vegetation. The vegetation can be present in either salt, brackish, or fresh water." Thus, some sites listed as grasslands can be arid, and others, even if surrounded by arid regions, can be wet by most definitions.

Patterns are hard to discern (Fig. 10). For two sites, $\Delta T \approx 6$ °C; one of them, with MAT < 0 °C, lies at an elevation of 4000 m in the northeastern part of the Tibetan Plateau (site FLX-CN-HaM), and the other, where MAT = 24 °C, is in arid central Australia (site FLX-AU-TTE, but for it, ΔT is based on only two years of data). For most of the remaining sites, 0 °C < ΔT < 4 °C. Mean values of ΔT are 2.1 \pm 1.5 °C for all 31 sites and 1.8 \pm 1.4 °C when only the 26 sites with MAT > 5 °C are included (Fig. 10A). The pattern seen with savannas that ΔT decreases with increasing precipitation gains little support (Fig. 10C).

Values of the Bowen ratio show large scatter but broadly increase with MAT (Fig. 10B), and they decrease with mean annual precipitation, although differently where MAT > 10 °C from where MAT < 10 °C (Fig. 10D).

Because of the apparently wet conditions at some of these sites but the absence of permanent wet surfaces of many grassy areas, drawing conclusions that could be applied to grassland paleoenvironments seems risky. By analogy with other regions, it makes sense to assume that for wet grasslands, $\Delta T \approx 1$ °C, but over semiarid grasslands, $\Delta T \approx 2-3$ °C. For example, Krishnan et al. (2012) reported values of $\Delta T = 2.5$ °C and 2.8 °C for two semiarid grasslands in Arizona, USA.

DISCUSSION AND CONCLUSIONS

The theory summarized above offers support for observations both of differences in surface, $T_{\rm s}$, and air, $T_{\rm a}$, temperatures, $\Delta T = T_{\rm s} - T_{\rm a}$, and of Bowen ratios, B, from the FLUXNET2015 data set, as well as published measurements of ΔT for warm seasons (e.g., Burgener et al., 2019; Kelson et al., 2020; Gallagher et al., 2019; Lu et al., 2019; Passey et al., 2010; Wang et al., 2020). Thus, the results presented here could be seen as providing theoretical justification augmented with additional data for what others have observed and inferred.

A couple of general patterns emerge when all data are considered together (Fig. 11). First, in regions of low temperature, values of ΔT can be especially large, >3 °C, and in some cases exceed 6 °C. In such regions, where during parts of the year the ground is frozen, sensible heat flux dominates the surface enthalpy flux. Accordingly, though with obvious exceptions, Bowen ratios are relatively large, B > 1. Moreover, because of the strong temperature dependence on specific humidity, values of both ΔT in Equation 11 and B in Equation 12 decrease as temperature increases, at least for -5 °C < MAT < 10-15 °C (Fig. 11). The scatter in data make the tendencies for ΔT and B to decrease with temperature crude, but these tendencies prevail for forests, shrublands, grasslands, and wetlands.

Geologically, these tendencies bear on past air temperatures at both high latitudes and high altitudes. High-latitude regions have undergone large swings in temperature of tens of degrees Celsius over geologic time, but temperatures in the tropics seem to have changed little. Thus, for periods when the poles were especially cold, estimates of soil temperatures risk overestimating the coldness of the air at high latitude. The measurement of soil temperatures offers an obvious tool for paleoaltimetry, but again, if high regions were especially cold, ignoring a difference between soil and air temperatures of, say, 4–5 °C could lead to an overestimate of paleoelevations of ~1000 m given that values of $|dT_a(z)/dz|$ can be ~4–5 °C/km. Moreover, simple theoretical arguments presented in Appendix B suggest that $d\Delta T(z)/dz$ can be 1–2 °C/km, which would enhance overestimates of past elevations if ΔT were ignored.

A second general pattern seen when all data are plotted (Fig. 11) is a tendency for ΔT to increase with MAT where MAT $\gtrsim 10$ °C, but measurements in savannas dominate this pattern. Clearer is tendency for ΔT and B to decrease with increasing precipitation. Although precipitation is an imperfect measure of aridity, the logic of these decreases with aridity is sensible. Where soil moisture is sparse, latent heat transfer is small compared with sensible heat transfer. Therefore, not only is the Bowen ratio large, but with most of the surface enthalpy flux carried by sensible heat, ΔT must be relatively large. This pattern is consistent with published measurements of ΔT made during summer (e.g., Burgener et al., 2019; Gallagher et al., 2019; Kelson et al., 2020; Lu et al., 2019; Passey et al., 2010; Wang et al., 2020).

It follows that where geologists can infer not just soil temperatures but also measures of aridity, they should be able to decide whether to assign $\Delta T \approx 1$ °C as for wet environments, or $\Delta T \gtrsim 3$ °C and possibly as much as 5–6 °C as for especially arid environments. Moreover, depending on land-surface cover,

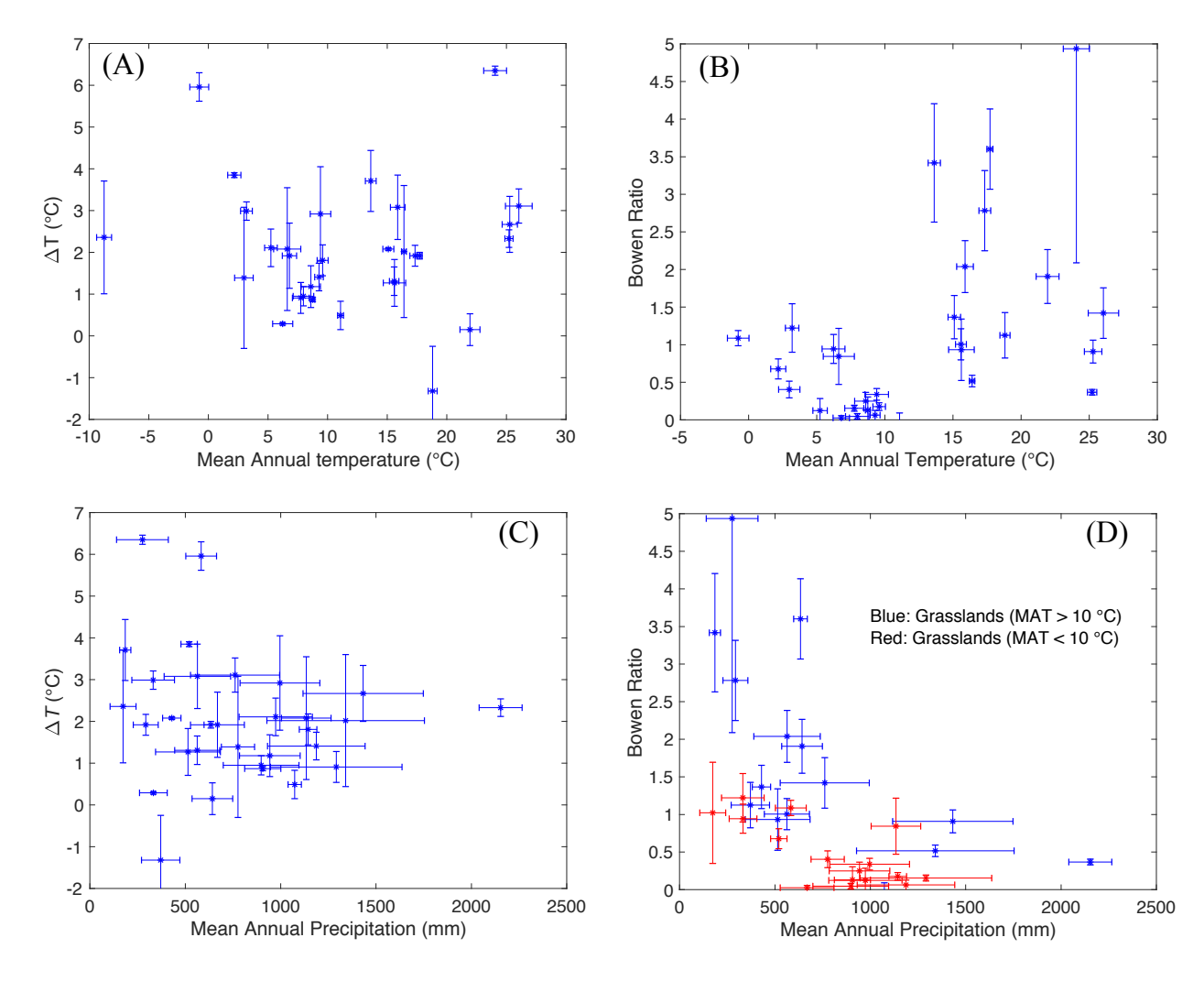


Figure 10. Results from the FLUXNET2015 database for grasslands. Error bars show standard deviations. (A) Values of ΔT , the difference between soil temperature, T_s , and that of the overlying air, T_a , versus mean annual temperatures, MAT. (B) Values of the Bowen ratio, B, versus MAT. (C) Values of ΔT versus mean annual precipitation. (D) Values of the Bowen ratio versus mean annual precipitation.

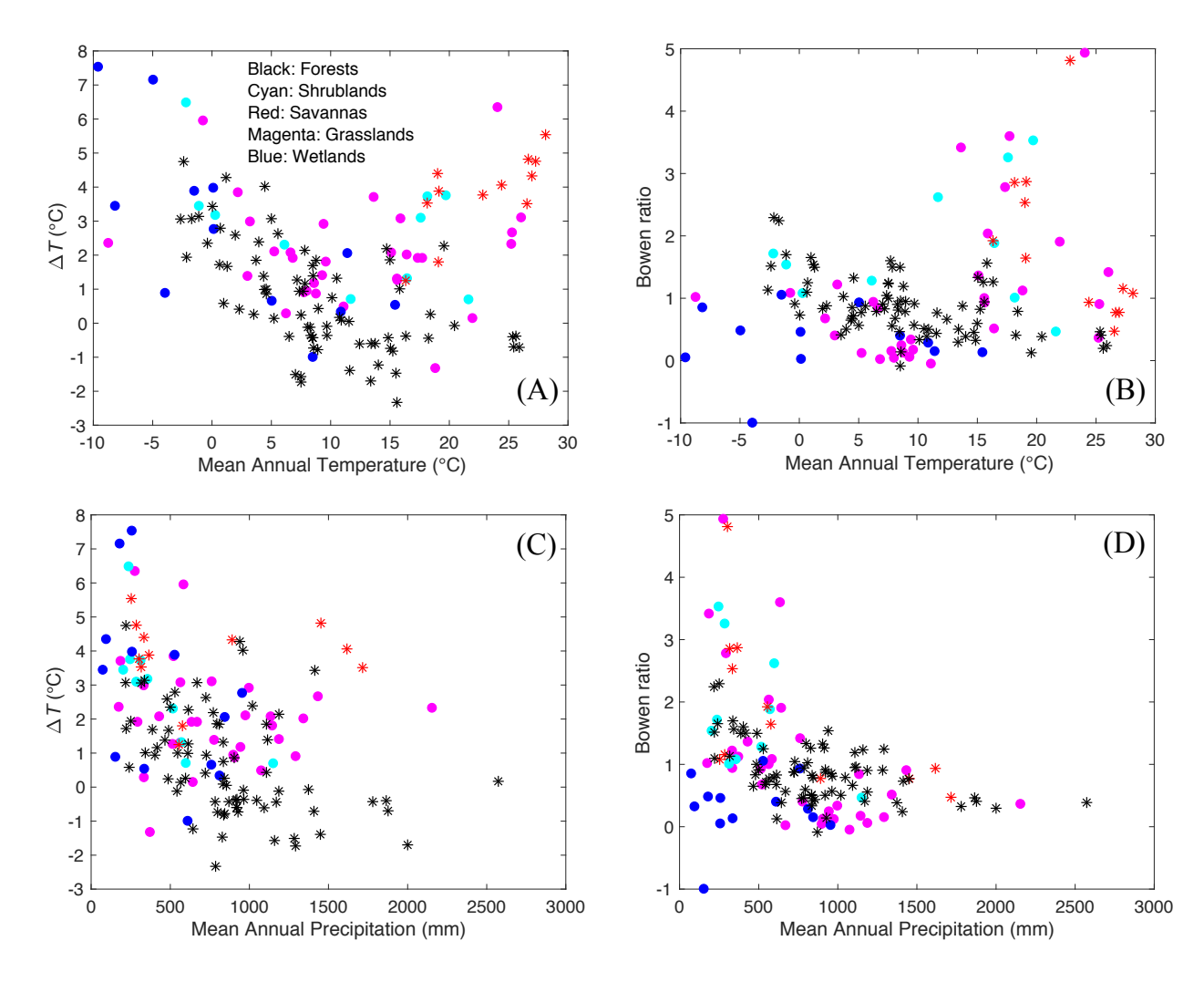


Figure 11. Results from the FLUXNET2015 database for all land cover types. (A) Values of ΔT , the difference between soil temperature, T_s , and that of the overlying air, T_a , versus mean annual temperatures, MAT. (B) Values of the Bowen ratio, B, versus MAT. (C) Values of ΔT versus mean annual precipitation. (D) Values of the Bowen ratio versus mean annual precipitation.

mean annual temperature (MAT), and aridity, subtler systematic patterns in values of ΔT and B emerge.

For wet environments, and wetlands in particular, albeit many of which are not likely to yield paleotemperatures of surface materials, latent heat dominates the surface enthalpy flux. FLUXNET2015 data are few, but for $T_a > 0$ °C, $\Delta T \approx 1$ °C (Figs. 6A and 11A) and Bowen ratios are small, B < 1 (Figs. 6B and 11B). As noted above, however, where the MAT < 0 °C, ΔT can be large, 4–6 °C (Figs. 6A and 11A). Because geologists measuring soil temperatures would determine whether or not such temperatures are low, $\lesssim 5$ °C, it follows that if they had other evidence that the deposits accumulated in a wetland environment, they would have the most important information needed to decide how to assign a value of ΔT .

For forests of different kinds, FLUXNET2015 data among forests of different kinds show similar patterns. For most, 0 °C < ΔT < 2 °C, but in cold environments (MAT \lesssim 5 °C), values of ΔT can reach 3–5 °C (Figs. 7A and 11A). Similarly, Bowen ratios decrease with increasing MAT and are consistent with a major role played by the increase of specific humidity, $q^*(T_a)$, in the denominator of the expression for B in Equation 12 with increasing temperature, T_a or MAT (Fig. 7B). If geologic evidence demonstrates a forest environment, then as with wetlands, determining whether ΔT < 2 °C or possibly 3–5 °C again follows principally from the inferred soil temperature.

The few FLUXNET2015 data for shrublands share features with those for wetlands and forests. Again, in cold environments, where MAT \lesssim 0 °C, ΔT can be relatively large, $\Delta T >$ 3 °C (Figs. 8 and 11). Comparable values of ΔT characterize some warm regions as well, and Bowen ratios crudely increase with MAT (Figs. 8B and 11B). Values of ΔT , and less clearly of Bowen ratios, decrease with increasing mean annual precipitation (Figs. 8C, 8D, 11C, and 11D), as expected with sensible heat transporting more of the surface enthalpy flux than latent heat in arid environments. Data may be too few to demonstrate that where mean annual precipitation is <500 mm, $\Delta T \approx$ 3–4 °C (Figs. 8C and 11C), but that suggestion seems a reasonable supposition for regions where paleoprecipitation can be constrained. If geologic evidence points to a shrubland environment and allows an inference of aridity, whether as paleoprecipitation or some other proxy, then from such an inference, choosing between estimates of $\Delta T \approx$ 3–5 °C or $\Delta T \approx$ 1 °C should be possible.

For savannas, woody or open, the FLUXNET2015 data set includes only relatively warm sites, MAT > 15 °C. For most, 3.5 °C < ΔT < 5.5 °C (Figs. 9A and 11A). Unlike for shrublands and forests, however, there is no obvious correlation with mean annual precipitation (Figs. 9C and 11C). Crudely, Bowen ratios decrease with increasing MAT, suggesting that, as for wetlands (Fig. 6B) and forests (Fig. 7B), the increase of specific humidity, $q^*(T_a)$, with increasing T_a or MAT affects the Bowen ratio most (Figs. 9B and 11B). The largest Bowen ratios, B > 2, also come from arid sites with low mean annual precipitation (<500 mm), but low precipitation does not require high B (Figs. 9D and 11D). If geologic evidence, from pollen for example, suggests a savanna environment, then assuming 3.5 °C < ΔT < 5.5 °C appears to be sensible.

Compared to the various other types of surface cover, FLUXNET2015 data for grasslands are many, but unfortunately, they do not reveal simple patterns.

Values of ΔT range from <0 °C to >6 °C, but most lie between 0 °C and 3 °C (Figs. 10A and 11A). Similarly, ΔT does not correlate with mean annual precipitation (Figs. 10C and 11C). Bowen ratios reveal slightly clearer patterns, with large values of B > 1.5 occurring only where MAT > 10 °C (Figs. 10B and 11B). If one separates sites with MAT < 10 °C from those with MAT > 10 °C, each group suggests decreasing values of Bowen ratios with increasing precipitation (Figs. 10D and 11D), as expected if moisture availability, β , most strongly affects the denominator of the expression for B in Equation 12. The lack of clear patterns for ΔT may arise because grasslands occur in a wide spectrum of environments, including high latitudes and alpine settings that are cold, wet settings and elsewhere in semiarid ones. The range of Bowen ratios for wet and semiarid grasslands (Table 4) suggests that values of ΔT may range from ~1 °C in wet environments to ~3 °C in arid ones. Thus, geologic inferences of grasslands might provide inadequate clues for inferring past values ΔT , and perhaps the safe assumption is simply that for past grasslands, ΔT = 1.5 ± 1.5 °C.

The FLUXNET2015 data set does not include sites from deserts, and perhaps only rare geological samples will come from ancient deserts. Nevertheless, the consistently large Bowen ratios over deserts, $B \gtrsim 4$ (Table 4), virtually assure large values of $\Delta T \approx 4$ –6 °C, as others have inferred (e.g., Burgener et al., 2019; Gallagher et al., 2019; Kelson et al., 2020; Lu et al., 2019; Passey et al., 2010; Wang et al., 2020).

In principle, geologists who infer past temperatures of soils and surface materials can determine not only paleotemperatures of the soil but also paleolatitudes for when such material was deposited and other aspects of past environments. In several environments—wetlands (Fig. 6), forests (Fig. 7), and shrublands (Fig. 8)—values of ΔT depend on mean annual temperatures, which in turn depend on latitudes. Thus, knowledge of both temperature and latitude should provide a guide in deciding what values of ΔT make sense.

A major factor influencing ΔT is tree cover, with values of ΔT tending to be greater over arid than wet regions and over those with grass cover than over forests and wetlands. Cerling et al. (2011) showed that at least for regions where C_4 plants grow, measurements of $\delta^{13}C$ in soils could be used to estimate the fraction of land covered by woody plants—trees and shrubs. Similarly, for where C_4 plants are part of the vegetation, Passey (2012) developed Kohn's (2010) suggestion that $\delta^{13}C$ values could be used to infer paleoprecipitation and showed that $\delta^{13}C$ in fossil mammal teeth offered promise. Lu et al. (2019) proposed using the total organic carbon content in the sediment containing the brGDGTs to estimate the amount of vegetation covering the region, with the assumption that more vegetations implies smaller ΔT . Fossil pollen as well as macrofossils can also discriminate among different types of forest, grass, and vegetation that thrives in arid environments. Thus, proxies of past environments offer clues for assigning values of ΔT in the different geologic settings.

In summary, theory and observation suggest the following for regions with MAT $\gtrsim 5$ °C: $\Delta T=1$ °C in wetlands, 1 \pm 1 °C in forests, 3–4 °C in shrublands, 4 \pm 1 °C in savannas, 1 °C in wet grasslands to 2–3 °C in arid grasslands, and 4–6 °C in deserts. Where MAT $\lesssim 5$ °C, we should expect $\Delta T>3$ °C and possibly $\Delta T>5$ °C (Fig. 11). Not only are these suggested values crude, but also

they apply to mean annual conditions. Values of ΔT vary over the seasonal cycle, and as geologists learn the extent to which inferences of past surface temperatures, $T_{\rm s}$, apply to different seasons, the ranges given above should undergo refinement.

APPENDIX A. LINEARIZATION OF THE LATENT HEAT FLUX ABOUT AIR TEMPERATURE, Ta

As described in basic texts (e.g., Pierrehumbert, 2010; Wallace and Hobbs, 1977), the specific humidity, q, is related to mixing ratio of vapor to dry air, $r = \rho_v/\rho_d$, by:

$$q = \frac{\rho_{v}}{\rho_{d} + \rho_{v}} = \frac{r}{1 + r} \approx r,\tag{A1}$$

where ρ_v and ρ_d are densities of vapor and dry air, respectively. The mixing ratio is given by:

$$r = \frac{e/R_vT}{P_v/R_vT} = \frac{ee}{P_v} \approx \frac{ee}{P},$$
 (A2)

where e and P_d are the partial pressures of vapor and dry air, respectively, R_v and R_d are gas constants for vapor and dry air, respectively, T is absolute temperature, $\mathbf{c} = 0.622$ is the ratio of molecular masses of vapor and the mixture of N_2 , O_2 , and trace gases in dry air, and $P = P_d + e$ is atmospheric pressure. From the Clausius-Clapeyron equation, the partial pressure of water vapor at saturation, e^* (in millibars or hectopascals), can be written as:

$$e*(T) = 6.112 \exp\left(\frac{L_{v}}{R_{v}T_{0}} - \frac{L_{v}}{R_{v}T}\right),$$
 (A3)

where T_0 = 273.16 K. Combining Equations A1, A2, and A3 then yields for specific humidity at saturation, $q^*(T)$:

$$q*(T) = \frac{6.112 \in}{P} \exp\left(\frac{L_{v}}{R_{v}T_{0}} - \frac{L_{v}}{R_{v}T}\right). \tag{A4}$$

Consider the difference in $q^*(T)$ between two temperatures not very different from one another, like T_a and $T_s = T_a + \Delta T$:

$$q*(T_a+\Delta T) = \frac{6.112 \in \text{exp}\left(\frac{L_v}{R_v T_0} - \frac{L_v}{R_v (T_a + \Delta T)}\right). \tag{A5}$$

It follows that:

$$q*(T_s) = q*(T_s + \Delta T) = q*(T_s) \left(1 + \frac{L_v}{R_v T_s^2} \Delta T + \dots\right).$$
 (A6)

For a common air temperature at the base of the troposphere, $T_a = 285$ °C, with $L_v = 2500$ kJ/kg and $R_v = 461$ J/(kg·K), $L_v/R_v T_a^2 \approx 0.07$ K⁻¹. Inserting Equation A6 with this relationship into Equation 8 yields the latent heat transfer given by Equation 9.

Because $q^*(T_a)$ varies inversely with pressure, it would increase with elevation if the decrease in T_a with elevation were ignored.

APPENDIX B. EFFECT OF ELEVATION ON $\Delta T = T_s - T_a$

Because $q^*(T)$, defined in Equation A5 or A6, depends on pressure, it also depends on elevation. For our purposes here, pressure can be approximated as $P(z) = P_0 e^{-zH}$, where $P_0 \approx 1000$ hPa is pressure at sea level and $H \approx 8$ km is the scale height (e.g., Wallace and Hobbs, 1977). To simplify Equation 11, let us rewrite it, using $q^*(T)$ defined in Equation A6, as:

$$\Delta T(z) = \frac{R_n(z) - \rho c_T |v| \beta L_y q^* (T_{a0} - \Gamma z) e^{z/H} [1 - RH]}{h},$$
(B1)

where $R_n(z) = S_{\bigcirc} (1-\alpha) - e_s e^* \sigma T_s^4$ is the net radiation at a surface at height z, $b_{\text{total}} = b_{\text{ir}} + b_{\text{sens}} + b_{\text{lat}}$ in the denominator of Equation 11 is treated as independent of height z, T_{a0} is the air temperature at sea level, and $\Gamma = |dT_a(z)/dz|$ treats the temperature of air just above surfaces at height z as decreasing linearly with surface elevation. Making the same approximation used in transforming Equation A5 to Equation A6 and again assuming that $L_v/R_vT_s^2 = 0.07 \text{ K}^{-1}$ yields:

$$\Delta T(z) = \frac{R_n(z) - \rho c_T |\nu| \beta L_\nu q^* (T_{a0}) e^{z/H} [1 - RH - 0.07\Gamma z]}{b_{\text{total}}}.$$
 (B2)

Differentiating Equation B2 with respect to height z yields:

$$\frac{d\Delta T(z)}{dz} = \frac{\frac{dR_{n}(z)}{dz} + \left(0.07\Gamma - \frac{1 - RH - 0.07\Gamma z}{H}\right)e^{z/H}\rho c_{T}|v|\beta L_{\nu}q^{*}(T_{a0})}{b_{cotal}}.$$
(B3)

The first term in the numerator of Equation B3, $dR_n(z)/dz$, is likely to be negative. Although the radiation balance at the top of the atmosphere is not equal to that at the surface, the same logic applied to one applies to the other. The thinner atmosphere above higher versus lower surfaces should increase $S_{\odot}(1-\alpha)$, and alone that increase would lead to a warmer surface at height. The thinner, colder atmosphere versus air over low terrain, however, would contain less greenhouse gas, and more longwave radiation from the surface would escape to space. In calculations of radiative-convective equilibrium, Hu and Boos (2017) found that a surface with pressure of 500 hPa, or at a height of -5.5 km, would receive ~7 W/m² more shortwave flux than one at 1000 hPa (or sea level), but outgoing longwave radiation would be reduced by 8 W/m² because of less CO₂ alone, an additional 9 W/m² because of less water vapor, and another 11 W/m² because of lower temperatures in black-body radiation associated with a steeper lapse rate over high versus low surfaces. We may treat the sum of ~21 W/m² over a height difference of 5.5 km as approximating $dR_n(z)/dz \approx -4$ W/m²/km.

To approximate the factor in parentheses times e^{zH} in the second term of Equation B3, let us assume RH = 0.6 and consider Γ = 2, 4, or 6 K/km at z = 0 and 5 km. That factor would increase from 0.09, 0.23, or 0.37 km $^{-1}$ at sea level to 0.18, 0.40, or 0.63 km $^{-1}$ at 5 km. With ranges of values of latent heat flux from -30 to -170 W/m 2 (Fig. 3), the magnitude of the second term in Equation B3 for cold regions with low latent heat flux seems unlikely to be less than the first term. For example, for latent heat fluxes of 50 or 150 W/m 2 and average values of the factor of 0.12 km $^{-1}$ for Γ = 2 K/km and of 0.5 km $^{-1}$ for Γ = 6 K/km, their products suggest values of 6 or 18 W/m 2 /km for Γ = 6 K/km, their products suggested values of $d \pi_0 (z)/dz \approx -4$ W/m 2 /km and using a denominator of $b_{\text{total}} \approx 50$ W/m 2 /K, expected values of $d \Delta T/dz$ would range from negligibly small to perhaps approaching 3 K/km. In one published example, Pérez-Angel et al. (2020) measured $d T_0 (z)/dz \approx 5.9$ K/km and $d \Delta T/dz \approx 0.7$ K/km. In another, along steep flanks of the Lajie Shan in northeastern Tibet, Wang and Liu (2021) measured $d T_0 (z)/dz \approx 3.9$ K/km but $d \Delta T/dz \approx 2.5$ K/km.

ACKNOWLEDGMENTS

I thank Paul Dirmeyer for help in accessing the FLUXNET2015 database, and B.E. Law and Shirley Papuga for help with specific sites. Lina Pérez-Angel read an early draft of the manuscript, and Weiguo Liu, Huanye Wang, and two anonymous reviewers offered many constructive comments that helped me improve the paper. The U.S. National Science Foundation supported this research through grants AGS-1740536, EAR-1929199, and ISE-1545859.

REFERENCES CITED

Al Nakshabandi, G., and Kohnke, H., 1965, Thermal conductivity and diffusivity of soils as related to moisture tension and other physical properties: Agricultural Meteorology, v. 2, p. 271–279, https://doi.org/10.1016/0002-1571(65)90013-0.

Anderson, R.S., 1998, Near-surface thermal profiles in alpine bedrock: Implications for the frost-weathering of rock: Arctic and Alpine Research, v. 30, p. 362–372, https://doi.org/10.2307/1552008

Anderson, R.S., and Anderson, S.P., 2010, Geomorphology: The Mechanics and Chemistry of Landscapes: Cambridge, UK, Cambridge University Press, 637 p., https://doi.org/10.1017 /CBO9780511794827.

Arain, M.A., Black, T.A., Barr, A.G., Griffis, T.J., Morgenstern, K., and Nesic, Z., 2003, Year-round observations of the energy and water vapour fluxes above a boreal black spruce forest: Hydrological Processes, v. 17, p. 3581–3600, https://doi.org/10.1002/hyp.1348.

Bagayoko, F., Yonkeu, S., Elbers, J., and van de Giesen, N., 2007, Energy partitioning over the West African savanna: Multi-year evaporation and surface conductance measurements in

- Eastern Burkina Faso: Journal of Hydrology (Amsterdam), v. 334, p. 545–559, https://doi.org/10.1016/j.jhydrol.2006.10.035.
- Baldocchi, D., and Ma, S., 2013, How will land use affect air temperature in the surface boundary layer? Lessons learned from a comparative study on the energy balance of an oak savanna and annual grassland in California, USA: Tellus B: Chemical and Physical Meteorology, v. 65, 19994, https://doi.org/10.3402/tellusb.v65i0.19994.
- Baldocchi, D.D., and Vogel, C.A., 1996, Energy and CO₂ flux densities above and below a temperate broad-leaved forest and a boreal pine forest: Tree Physiology, v. 16, p. 5–16, https://doi.org/10.1093/treephys/16.1-2.5.
- Baldocchi, D.D., and Xu, L., 2007, What limits evaporation from Mediterranean oak woodlands— The supply of moisture in the soil, physiological control by plants or the demand by the atmosphere?: Advances in Water Resources, v. 30, p. 2113–2122, https://doi.org/10.1016/j advwatres.2006.06.013.
- Baldocchi, D.D., Vogel, C.A., and Hall, B., 1997, Seasonal variation of energy and water vapor exchange rates above and below a boreal jack pine forest canopy: Journal of Geophysical Research, v. 102, p. 28,939–28,951, https://doi.org/10.1029/96JD03325.
- Baldocchi, D.D., Law, B.E., and Anthoni, P.M., 2000, On measuring and modeling energy fluxes above the floor of a homogeneous and heterogeneous conifer forest: Agricultural and Forest Meteorology, v. 102, p. 187–206, https://doi.org/10.1016/S0168-1923(00)00098-8.
- Baldocchi, D., Falge, E., Gu, L., Olson R., Hollinger, D., Running, S., Anthoni, P., Bernhofer, C., Davis, K., Evans, R., Fuentes, J., Goldstein, A., Katul, G., Law, J.B., Lee, X., Malhi, Y., Meyers, T., Munger, W., Oechel, W., Paw U, K.T., Pilegaard, K., Schmid, H.P., Valentini, R., Verma, S., Vesala, T., Wilson, K., and Wofsy, S., 2001, FLUXNET: A new tool to study the temporal and spatial variability of ecosystem-scale carbon dioxide, water vapor, and energy flux densities: Bulletin of the American Meteorological Society, v. 82, p. 2415–2434, https://doi.org/10.1175/1520-0477(2001)082<2415:FANTTS>2.3.CO;2.
- Baldocchi, D.D., Xu, L., and Kiang, N., 2004, How plant functional-type, weather, seasonal drought, and soil physical properties alter water and energy fluxes of an oak-grass savanna and an annual grassland: Agricultural and Forest Meteorology, v. 123, p. 13–39, https://doi.org/10.1016/j.agrformet.2003.11.006.
- Baldocchi, D., Chen, Q., Chen, X., Ma, S., Miller, G., Ryu, Y., Xiao, J., Wenk, R., and Battles, J., 2010, The dynamics of energy, water, and carbon fluxes in a blue oak (*Quercus douglasii*) savanna in California, in Hill, M.J., and Hanan, N.P., eds., Ecosystem Function in Savannas: Boca Raton, Florida, CRC Press, p. 135–151, https://doi.org/10.1201/b10275-16.
- Baldocchi, D., Ma, S., and Verfaillie, J., 2021, On the inter- and intra-annual variability of ecosystem evapotranspiration and water use efficiency of an oak savanna and annual grassland subjected to booms and busts in rainfall: Global Change Biology, v. 27, p. 359–375, https://doi.org/10.1111/gcb.15414.
- Bartlett, M.G., Chapman, D.S., and Harris, R.N., 2006, A decade of ground-air temperature tracking at Emigrant Pass Observatory, Utah: Journal of Climate, v. 19, p. 3722–3731, https://doi.org/10.1175/JCLI3808.1.
- Beringer, J., Chapin, F.S., III, Thompson, C.G., and McGuire, A.D., 2005, Surface energy exchanges along a tundra-forest transition and feedbacks to climate: Agricultural and Forest Meteorology, v. 131, p. 143–161, https://doi.org/10.1016/j.agrformet.2005.05.006.
- Betts, A.K., 2000, Idealized model for equilibrium boundary layer over land: Journal of Hydrometeorology, v. 1, p. 507–523, https://doi.org/10.1175/1525-7541(2000)001<0507:IMFEBL>2 .0.CO;2.
- Betts, A.K., Goulden, M., and Wofsy, S., 1999, Controls on evaporation in a boreal spruce forest: Journal of Climate, v. 12, p. 1601–1618, https://doi.org/10.1175/1520-0442(1999)012<1601: COEIAB>2.0.CO;2.
- Blanken, P.D., Black, T.A., Yang, P.C., Neumann, H.H., Nesic, Z., Staebler, R., den Hartog, G., Novak, M.D., and Lee, X., 1997, Energy balance and surface conductance of a boreal aspen forest: Partitioning overstory and understory components: Journal of Geophysical Research, v. 102, p. 28,915–28,927, https://doi.org/10.1029/97JD00193.
- Breecker, D.O., Sharp, Z.D., and McFadden, L.D., 2009, Seasonal bias in the formation and stable isotopic composition of pedogenic carbonate in modern soils from central New Mexico, USA: Geological Society of America Bulletin, v. 121, p. 630–640, https://doi.org/10.1130/B26413.1.
- Burgener, L., Huntington, K.W., Hoke, G.D., Schauer, A., Ringham, M.C., Latorre, C., and Díaz, F.P., 2016, Variations in soil carbonate formation and seasonal bias over >4 km of relief in the western Andes (30°S) revealed by clumped isotope thermometry: Earth and Planetary Science Letters, v. 441, p. 188–199, https://doi.org/10.1016/j.epsl.2016.02.033.

- Burgener, L.K., Huntington, K.W., Sletten, R., Watkins, J.M., Quade, J., and Hallet, B., 2018, Clumped isotope constraints on equilibrium carbonate formation and kinetic isotope effects in freezing soils: Geochimica et Cosmochimica Acta, v. 235, p. 402–430, https://doi.org/10.1016/j.gca .2018.06.006.
- Burgener, L.K., Hyland, E.G., Huntington, K.W., Kelson, J.R., and Sewall, J.O., 2019, Revisiting the equable climate problem during the Late Cretaceous greenhouse using paleosol carbonate clumped isotope temperatures from the Campanian of the Western Interior Basin, USA: Palaeogeography, Palaeoclimatology, Palaeoecology, v. 516, p. 244–267, https://doi.org/10 .1016/j.palaeo.2018.12.004.
- Cayan, D.R., 1980, Large-scale relationships between sea surface temperature and surface air temperature: Monthly Weather Review, v. 108, p. 1293–1301, https://doi.org/10.1175/1520-0493 (1980)108<1293:LSRBSS>2.0.CO:2.
- Cerling, T.E., Wynn, J.G., Andanje, S.A., Bird, M.I., Korir, D.K., Levin, N.E., Mace, W., Macharia, A.N., Quade, J., and Remien, C.H., 2011, Woody cover and hominin environments in the past 6 million years: Nature, v. 476, p. 51–56, https://doi.org/10.1038/nature10306.
- Chen, S., Chen, J., Lin, G., Zhang, W., Miao, H., Wei, L., Huang, J., and Han, X., 2009, Energy balance and partition in Inner Mongolia steppe ecosystems with different land use types: Agricultural and Forest Meteorology, v. 149, p. 1800–1809, https://doi.org/10.1016/j.agrformet .2009.06.009.
- Colcord, D.E., Cadieux, S.B., Brassell, S.C., Castañeda, I.S., Pratt, L.M., and White, J.R., 2015, Assessment of branched GDGTs as temperature proxies in sedimentary records from several small lakes in southwestern Greenland: Organic Geochemistry, v. 82, p. 33–41, https://doi.org/10.1016/j.orggeochem.2015.02.005.
- Cronin, T.W., 2013, A sensitivity theory for the equilibrium boundary layer over land: Journal of Advances in Modeling Earth Systems, v. 5, p. 764–784, https://doi.org/10.1002/jame.20048.
- Dang, X., Ding, W., Yang, H., Pancost, R.D., Naafs, B.D.A., Xue, J., Lin, X., Lu, J., and Xie, S., 2018, Different temperature dependence of the bacterial brGDGT isomers in 35 Chinese lake sediments compared to that in soils: Organic Geochemistry, v. 119, p. 72–79, https://doi.org/10 .1016/j.orggeochem.2018.02.008.
- da Rocha, H.R., Goulden, M.L., Miller, S.D., Menton, M.C., Pinto, L.D.V.O., de Freitas, H.C., and Silva Figueira, A.M., 2004, Seasonality of water and heat fluxes over a tropical forest in eastern Amazonia: Ecological Applications, v. 14, p. 22–32, https://doi.org/10.1890/02-6001.
- De Jonge, C., Hopmans, E.C., Zell, C.I., Kim, J.H., Schouten, S., and Sinninghe Damsté, J.S., 2014, Occurrence and abundance of 6-methyl branched glycerol dialkyl glycerol tetraethers in soils: Implications for palaeoclimate reconstruction: Geochimica et Cosmochimica Acta, v. 141, p. 97–112, https://doi.org/10.1016/j.gca.2014.06.013.
- den Hartog, G., Neumann, H.H., King, K.M., and Chipanshi, A.C., 1994, Energy budget measurements using eddy correlation and Bowen ratio techniques at the Kinosheo Lake tower site during the Northern Wetlands Study: Journal of Geophysical Research, v. 99, p. 1539–1549, https://doi.org/10.1029/93JD00032.
- Donohoe, A., and Battisti, D.S., 2011, Atmospheric and surface contributions to planetary albedo: Journal of Climate, v. 24, p. 4402–4418, https://doi.org/10.1175/2011JCLl3946.1.
- Eiler, J.M., 2007, "Clumped-isotope" geochemistry—The study of naturally-occurring, multiply-substituted isotopologues: Earth and Planetary Science Letters, v. 262, p. 309–327, https://doi.org/10.1016/j.epsl.2007.08.020.
- Eugster, W., Rouse, W.R., Pielke, R.A., Sr., Mcfadden, J.P., Baldocchi, D.D., Kittel, T.G.F., Chapin, F.S., Ill, Liston, G.E., Vidale, P.L., Vaganov, E., and Chambers, S., 2000, Land-atmosphere energy exchange in Arctic tundra and boreal forest: Available data and feedbacks to climate: Global Change Biology, v. 6, Suppl. 1, p. 84–115, https://doi.org/10.1046/j.1365-2486.2000.06015.x.
- Gallagher, T.M., and Sheldon, N.D., 2016, Combining soil water balance and clumped isotopes to understand the nature and timing of pedogenic carbonate formation: Chemical Geology, v. 435, p. 79–91, https://doi.org/10.1016/j.chemgeo.2016.04.023.
- Gallagher, T.M., Hren, M., and Sheldon, N.D., 2019, The effect of soil temperature seasonality on climate reconstructions from paleosols: American Journal of Science, v. 319, p. 549–581, https://doi.org/10.2475/07.2019.02.
- Ghosh, P., Adkins, J., Affek, H., Balta, B., Guo, W., Schauble, E.A., Schrag, D., and Eiler, J.M., 2006a, ¹³C-¹⁸O bonds in carbonate minerals: A new kind of paleothermometer: Geochimica et Cosmochimica Acta, v. 70, p. 1439–1456, https://doi.org/10.1016/j.gca.2005.11.014.
- Ghosh, P., Garzione, C.N., and Eiler, J.M., 2006b, Rapid uplift of the Altiplano revealed through ¹³C-¹⁸O bonds in paleosol carbonates: Science, v. 311, p. 511–515, https://doi.org/10.1126/science.1119365.

- Grünwald, T., and Bernhofer, C., 2007, A decade of carbon, water and energy flux measurements of an old spruce forest at the Anchor Station Tharandt: Tellus, v. 59B, p. 387–396, https://doi.org/10.1111/j.1600-0889.2007.00259.x.
- Gu, S., Tang, Y., Cui, X., Kato, T., Du, M., Li, Y., and Zhao, X., 2005, Energy exchange between the atmosphere and a meadow ecosystem on the Qinghai-Tibetan Plateau: Agricultural and Forest Meteorology, v. 129, p. 175–185, https://doi.org/10.1016/j.agrformet.2004.12.002.
- Günther, F., Thiele, A., Gleixner, G., Xu, B., Yao, T., and Schouten, S., 2014, Distribution of bacterial and archaeal ether lipids in soils and surface sediments of Tibetan lakes: Implications for GDGT-based proxies in saline high mountain lakes: Organic Geochemistry, v. 67, p. 19–30, https://doi.org/10.1016/j.orggeochem.2013.11.014.
- Hao, Y., Wang, Y., Huang, X., Cui, X., Zhou, X., Wang, S., Niu, H., and Jiang, G., 2007, Seasonal and interannual variation in water vapor and energy exchange over a typical steppe in Inner Mongolia, China: Agricultural and Forest Meteorology, v. 146, p. 57–69, https://doi.org/10 .1016/j.agrformet.2007.05.005.
- Hicks, B.B., and Hess, G.D., 1977, On the Bowen ratio and surface temperature at sea: Journal of Physical Oceanography, v. 7, p. 141–145, https://doi.org/10.1175/1520-0485(1977)007<0141:OTBRAS>2.0.CO;2.
- Hopmans, E.C., Weijers, J.W.H., Schefuß, E., Herfort, L., Sinninghe Damsté, J.S., and Schouten, S., 2004, A novel proxy for terrestrial organic matter in sediments based on branched and isoprenoid tetraether lipids: Earth and Planetary Science Letters, v. 224, p. 107–116, https:// doi.org/10.1016/j.epsl.2004.05.012.
- Hough, B.G., Fan, M., and Passey, B.H., 2014, Calibration of the clumped isotope geothermometer in soil carbonate in Wyoming and Nebraska, USA: Implications for paleoelevation and paleoclimate reconstruction: Earth and Planetary Science Letters, v. 391, p. 110–120, https://doi.org/10.1016/j.epsl.2014.01.008.
- Hsu, S.A., 1998, A relationship between the Bowen ratio and sea-air temperature difference under unstable conditions at sea: Journal of Physical Oceanography, v. 28, p. 2222–2226, https://doi .org/10.1175/1520-0485(1998)028<2222:ARBTBR>2.0.CO;2.
- Hu, S., and Boos, W.R., 2017, The physics of orographic elevated heating in radiative-convective equilibrium: Journal of the Atmospheric Sciences, v. 74, p. 2949–2965, https://doi.org/10.1175 //IAS_D.13.2.1
- Humphreys, E.R., Black, T.A., Ethier, G.J., Drewitt, G.B., Spittlehouse, D.L., Jork, E.-M., Nesic, Z., and Livingston, N.J., 2003, Annual and seasonal variability of sensible and latent heat fluxes above a coastal Douglas-fir forest, British Columbia, Canada: Agricultural and Forest Meteorology, v. 115, p. 109–125, https://doi.org/10.1016/S0168-1923(02)00171-5.
- Huntington, K.W., Wernicke, B.P., and Eiler, J.M., 2010, Influence of climate change and uplift on Colorado Plateau paleotemperatures from carbonate clumped isotope thermometry: Tectonics, v. 29, TC3005, https://doi.org/10.1029/2009TC002449.
- Huth, T.E., Cerling, T.E., Marchetti, D.W., Bowling, D.R., Ellwein, A.L., and Passey, B.H., 2019, Seasonal bias in soil carbonate formation and its implications for interpreting high-resolution paleoarchives: Evidence from southern Utah: Journal of Geophysical Research: Biogeosciences, v. 124, p. 616–632, https://doi.org/10.1029/2018JG004496.
- Kelliher, F.M., Leuning, R., Raupach, M.R., and Schulze, E.-D., 1995, Maximum conductances for evaporation from global vegetation types: Agricultural and Forest Meteorology, v. 73, p. 1–16, https://doi.org/10.1016/0168-1923(94)02178-M.
- Kelliher, F.M., Lloyd, J., Arneth, A., Byers, J.N., McSeveny, T.M., Milukova, I., Grigoriev, S., Panfyorov, M., Sogatchev, A., Verlargin, A., Ziegler, W., Bauer, G., and Schulze, E.-D., 1998, Evaporation from a central Siberian pine forest: Journal of Hydrology (Amsterdam), v. 205, p. 279–296, https://doi.org/10.1016/S0022-1694(98)00082-1.
- Kelson, J.R., Huntington, K.W., Breecker, D.O., Burgener, L.K., Gallagher, T.M., Hoke, G.D., and Petersen, S.V., 2020, A proxy for all seasons? A synthesis of clumped isotope data from Holocene soil carbonates: Quaternary Science Reviews, v. 234, 106259, https://doi.org/10 .1016/j.quascirev.2020.106259.
- Kohn, M.J., 2010, Carbon isotope compositions of terrestrial C3 plants as indicators of (paleo) ecology and (paleo)climate: Proceedings of the National Academy of Sciences of the United States of America, v. 107, p. 19,691–19,695, https://doi.org/10.1073/pnas.1004933107.
- Kondo, J., 1976, Heat balance of the East China Sea during the Air Mass Transformation Experiment: Journal of the Meteorological Society of Japan, v. 54, p. 382–398, https://doi.org/10.2151/jmsj1965.54.6_382.
- Krishnan, P., Meyers, T.P., Scott, R.L., Kennedy, L., and Heuer, M., 2012, Energy exchange and evapotranspiration over two temperate semi-arid grasslands in North America: Agricultural and Forest Meteorology, v. 153, p. 31–44, https://doi.org/10.1016/j.agrformet.2011.09.017.

- Launiainen, S., 2010, Seasonal and inter-annual variability of energy exchange above a boreal Scots pine forest: Biogeosciences, v. 7, p. 3921–3940, https://doi.org/10.5194/bg-7-3921-2010.
- Laymon, C.A., and Quattrochi, D.A., 2004, Estimating spatially distributed surface fluxes in a semi-arid Great-Basin desert using Landsat TM thermal data, in Quattrochi, D.A., and Luvall, J.C., eds., Thermal Remote Sensing in Land Surface Processes: Boca Raton, Florida, CRC Press, p. 133–159.
- Li, J., Pancost, R.D., Naafs, B.D.A., Yang, H., Zhao, C., and Xie, S., 2016, Distribution of glycerol dialkyl glycerol tetraether (GDGT) lipids in a hypersaline lake system: Organic Geochemistry, v. 99, p. 113–124, https://doi.org/10.1016/j.orggeochem.2016.06.007.
- Li, J., Naafs, B.D.A., Pancost, R.D., Yang, H., Liu, D., and Xie, S., 2017, Distribution of branched tetraether lipids in ponds from Inner Mongolia, NE China: Insight into the source of brGDGTs: Organic Geochemistry, v. 112, p. 127–136, https://doi.org/10.1016/j.orggeochem.2017.07.005.
- Li, M., Babel, W., Chen, X., Zhang, L., Sun, F., Wang, B., Ma, Y., Hu, Z., and Foken, T., 2015, A 3-year dataset of sensible and latent heat fluxes from the Tibetan Plateau, derived using eddy covariance measurements: Theoretical and Applied Climatology, v. 122, p. 457–469, https://doi.org/10.1007/s00704-014-1302-0.
- Li, S.-G., Lai, C.-T., Lee, G., Shimoda, G., Yokoyama, S., Higuchi, T., and Oikawa, A., 2005, Evapotranspiration from a wet temperate grassland and its sensitivity to microenvironmental variables: Hydrological Processes, v. 19, p. 517–532, https://doi.org/10.1002/hyp.5673.
- Li, S.-G., Eugster, W., Asanuma, J., Kotani, A., Davaa, G., Oyunbaatar, D., and Sugita, M., 2006, Energy partitioning and its biophysical control above a grazing steppe in central Mongolia: Agricultural and Forest Meteorology, v. 137, p. 89–106, https://doi.org/10.1016/j.agrformet .2006.03.010.
- Loomis, S.E., Russell, J.M., and Sinninghe Damsté, J.S., 2011, Distributions of branched GDGTs in soils from western Uganda and implications for a lacustrine paleothermometer: Organic Geochemistry, v. 42, p. 739–751, https://doi.org/10.1016/j.orgaeochem.2011.06.004.
- Lu, H., Liu, W., Yang, H., Wang, H., Liu, Z., Leng, Q., Sun, Y., Zhou, W., and An, Z., 2019, 800-kyr land temperature variations modulated by vegetation changes on Chinese Loess Plateau: Nature Communications, v. 10, 1958, https://doi.org/10.1038/s41467-019-09978-1.
- Ma, N., Zhang, Y., Guo, Y., Gao, H., Zhang, H., and Wang, Y., 2015, Environmental and biophysical controls on the evapotranspiration over the highest alpine steppe: Journal of Hydrology (Amsterdam), v. 529, p. 980–992, https://doi.org/10.1016/j.jhydrol.2015.09.013.
- Ma, S., Baldocchi, D.D., Wolf, S., and Verfaillie, J., 2016, Slow ecosystem responses conditionally regulate annual carbon balance over 15 years in Californian oak-grass savanna: Agricultural and Forest Meteorology, v. 228–229, p. 252–264, https://doi.org/10.1016/j.agrformet.2016.07.016.
- Majozi, N.P., Mannaerts, C.M., Ramoelo, A., Mathieu, R., Nickless, A., and Verhoef, W., 2017, Analysing surface energy balance closure and partitioning over a semi-arid savanna FLUXNET site in Skukuza, Kruger National Park, South Africa: Hydrology and Earth System Sciences, v. 21, p. 3401–3415, https://doi.org/10.5194/hess-21-3401-2017.
- Malek, E., Bingham, G.E., and McCurdy, G.D., 1990, Evapotranspiration from the margin and moist playa of a closed desert valley: Journal of Hydrology (Amsterdam), v. 120, p. 15–34, https://doi.org/10.1016/0022-1694(90)90139-O.
- Martínez-Sosa, P., Tierney, J.E., Stefanescu, I.C., Dearing Crampton-Flood, E., Shuman, B.N., and Routson, C., 2021, A global Bayesian temperature calibration for lacustrine brGDGTs: Geochimica et Cosmochimica Acta, v. 305, p. 87–105, https://doi.org/10.1016/j.gca.2021.04.038.
- McColl, K.A., 2020, Practical and theoretical benefits of an alternative to the Penman-Monteith evapotranspiration equation: Water Resources Research, v. 56, e2020WR027106, https://doi.org/10.1029/2020WR027106.
- Miralles, D.G., De Jeu, R.A.M., Gash, J.H., Holmes, T.R.H., and Dolman, A.J., 2011, Magnitude and variability of land evaporation and its components at the global scale: Hydrology and Earth System Sciences, v. 15, p. 967–981, https://doi.org/10.5194/hess-15-967-2011.
- Miralles, D.G., Brutsaert, W., Dolman, A.J., and Gash, J.H., 2020, On the use of the term "evapotranspiration": Water Resources Research, v. 56, e2020WR028055, https://doi.org/10.1029/2020WR028055.
- Monteith, J.L., 1965, Evaporation and environment: Symposia of the Society for Experimental Biology, v. 19, p. 205–234.
- Oke, T.R., 1987, Boundary Layer Climates (second edition): London, Methuen & Co. Ltd., 435 p.
- Oliphant, A.J., Grimmond, C.S.B., Zutter, H.N., Schmid, H.P., Su, H.-B., Scott, S.L., Offerle, B., Randolph, J.C., and Ehman, J., 2004, Heat storage and energy balance fluxes for a temperate deciduous forest: Agricultural and Forest Meteorology, v. 126, p. 185–201, https://doi.org/10.1016/j.agrformet.2004.07.003.

- Passey, B.H., 2012, Reconstructing terrestrial environments using stable isotopes in fossil teeth and paleosol carbonates, in Ivany, L.C., and Huber, B., eds., Reconstructing Earth's Deep-Time Climate—The State of the Art in 2012: Paleontological Society Papers 18, p. 167–194, https:// doi.org/10.1017/S1089332600002606.
- Passey, B.H., Levin, N.E., Cerling, T.E., Brown, F.H., and Eiler, J.M., 2010, High-temperature environments of human evolution in East Africa based on bond ordering in paleosol carbonates: Proceedings of the National Academy of Sciences of the United States of America, v. 107, p. 11,245–11,249, https://doi.org/10.1073/pnas.1001824107.
- Pastorello, G., et al., 2020, The FLUXNET2015 dataset and the ONEFlux processing pipeline for eddy covariance data: Scientific Data, v. 7, 225, https://doi.org/10.1038/s41597-020-0534-3.
- Pérez-Angel, L.C., Sepúlveda, J., Molnar, P., Montes, C., Rajagopalan, B., Snell, K., Gonzalez-Arango, C., and Dildar, N., 2020, Soil and air temperature calibrations using branched GDGTs for the tropical Andes of Colombia: Toward a pan-tropical calibration: Geochemistry, Geophysics, Geosystems, v. 21, e2020GC008941, https://doi.org/10.1029/2020GC008941.
- Peters, N.A., Huntington, K.W., and Hoke, G.D., 2013, Hot or not? Impact of seasonally variable soil carbonate formation on paleotemperature and O-isotope records from clumped isotope thermometry: Earth and Planetary Science Letters, v. 361, p. 208–218, https://doi.org/10.1016/j.epsl.2012.10.024.
- Pierrehumbert, R.T., 2010, Principles of Planetary Climate: Cambridge, UK, Cambridge University Press, 652 p., https://doi.org/10.1017/CBO9780511780783.
- Pond, S., Phelps, G.T., Paquin, J.E., McBean, G., and Stewart, R.W., 1971, Measurements of the turbulent fluxes of momentum, moisture and sensible heat over the ocean: Journal of the Atmospheric Sciences, v. 28, p. 901–917, https://doi.org/10.1175/1520-0469(1971)028<0901: MOTTFO>2.0.CO;2.
- Quade, J., Garzione, C., and Eiler, J., 2007, Paleoelevation reconstruction using pedogenic carbonates: Reviews in Mineralogy and Geochemistry, v. 66, p. 53–87, https://doi.org/10.2138/rmg.2007.66.3.
- Quade, J., Eiler, J., Daëron, M., and Achyuthan, H., 2013, The clumped isotope geothermometer in soil and paleosol carbonate: Geochimica et Cosmochimica Acta, v. 105, p. 92–107, https://doi.org/10.1016/j.gca.2012.11.031.
- Raberg, J.H., Harning, D.J., Crump, S.E., de Wet, G., Blumm, A., Kopf, S., Geirsdóttir, Á., Miller, G.H., and Sepúlveda, J., 2021, Revised fractional abundances and warm-season temperatures substantially improve brGDGT calibrations in lake sediments: Biogeosciences, v. 18, p. 3579–3603, https://doi.org/10.5194/bq-18-3579-2021.
- Rao, G.R.L., Rao, M.V., Prasad, P.H., and Reddy, K.G., 1986, Distribution of Bowen ratio over the Indian Ocean: Mausam (New Delhi), v. 37, p. 71–72.
- Raupach, M.R., 1995, Vegetation-atmosphere interaction and surface conductance at leaf and regional scales: Agricultural and Forest Meteorology, v. 73, p. 151–179, https://doi.org/10.1016/0168-1923(94)05071-D.
- Ringham, M.C., Hoke, G.D., Huntington, K.W., and Aranibar, J.N., 2016, Influence of vegetation type and site-to-site variability on soil carbonate clumped isotope records, Andean piedmont of Central Argentina (32–34°S): Earth and Planetary Science Letters, v. 440, p. 1–11, https://doi.org/10.1016/j.epsl.2016.02.003.
- Roupsard, O., Bonnefond, J.-M., Irvine, M., Berbigier, P., Nouvellon, Y., Dauzat, J., Taga, S., Hamel, O., Jourdan, C., Saint-André, L., Mialet-Serra, I., Labouisse, J.-P, Epron, D., Joffre, R., Braconnier, S., Rouzière, A., Navarro, M., and Bouillet, J.-P, 2006, Partitioning energy and evapo-transpiration above and below a tropical palm canopy: Agricultural and Forest Meteorology, v. 139, p. 252–268, https://doi.org/10.1016/j.agrformet.2006.07.006.
- Rubino, A., Zanchettin, D., De Rovere, F., and McPhaden, M.J., 2020, On the interchangeability of sea-surface and near-surface air temperature anomalies in climatologies: Scientific Reports, v. 10, 7433, https://doi.org/10.1038/s41598-020-64167-1.
- Russell, J.M., Hopmans, E.C., Loomis, S.E., Liang, J., and Sinninghe Damsté, J.S., 2018, Distributions of 5- and 6-methyl branched glycerol dialkyl glycerol tetraethers (brGDGTs) in East African lake sediment: Effects of temperature, pH, and new lacustrine paleotemperature calibrations: Organic Geochemistry, v. 117, p. 56–69, https://doi.org/10.1016/j.orggeochem.2017.12.003.
- Ryu, Y., Baldocchi, D.D., Ma, S., and Hehn, T., 2008, Interannual variability of evapotranspiration and energy exchange over an annual grassland in California: Journal of Geophysical Research, v. 113, D09104, https://doi.org/10.1029/2007JD009263.
- Snell, K.E., Thrasher, B.L., Eiler, J.M., Koch, P.L., Sloan, L.C., and Tabor, N.J., 2013, Hot summers in the Bighorn Basin during the early Paleogene: Geology, v. 41, p. 55–58, https://doi.org/10 .1130/G33567.1.

- Sommer, R., de Abreu Sá, T.D., Vielhauer, K., Carioca de Araújo, A., Fölster, H., and Vlek, P.L.G., 2002, Transpiration and canopy conductance of secondary vegetation in the eastern Amazon: Agricultural and Forest Meteorology, v. 112, p. 103–121, https://doi.org/10.1016/S0168 -1923(02)00044-8.
- Stewart, J.B., and Thom, A.S., 1973, Energy budgets in pine forest: Quarterly Journal of the Royal Meteorological Society, v. 99, p. 154–170, https://doi.org/10.1002/gi.49709941913.
- Sturman, A.P., and McGowan, H.A., 2009, Observations of dry season surface energy exchanges over a desert clay pan, Queensland, Australia: Journal of Arid Environments, v. 73, p. 74–81, https://doi.org/10.1016/j.jaridenv.2008.08.008.
- Sun, G., Noormets, A., Gavazzi, M.J., McNulty, S.G., Chen, J., Domec, J.-C., King, J.S., Amatya, D.M., and Skaggs, R.W., 2010, Energy and water balance of two contrasting loblolly pine plantations on the lower coastal plain of North Carolina, USA: Forest Ecology and Management, v. 259, p. 1299–1310, https://doi.org/10.1016/j.foreco.2009.09.016.
- Tang, Y., Wen, X., Sun, X., and Wang, H., 2014, Interannual variation of the Bowen ratio in a sub-tropical coniferous plantation in southeast China, 2003–2012: PLoS One, v. 9, e88267, https://doi.org/10.1371/journal.pone.0088267.
- Tierney, J.E., and Russell, J.M., 2009, Distributions of branched GDGTs in a tropical lake system: Implications for lacustrine application of the MBT/CBT paleoproxy: Organic Geochemistry, v. 40, p. 1032–1036, https://doi.org/10.1016/j.orggeochem.2009.04.014.
- van Bree, L.G.J., Peterse, F., Baxter, A.J., De Crop, W., van Grinsven, S., Villanueva, L., Verschuren, D., and Sinninghe Damsté, J.S., 2020, Seasonal variability and sources of in situ brGDGT production in a permanently stratified African crater lake: Biogeosciences, v. 17, p. 5443–5463, https://doi.org/10.5194/bg-17-5443-2020.
- Verhoef, A., 1995, Surface energy balance of shrub vegetation in the Sahel [Ph.D. thesis]: Wageningen, Netherlands, Wageningen Agricultural University, 247 p.
- Verhoef, A., Allen, S.J., and Lloyd, C.R., 1999, Seasonal variation of surface energy balance over two Sahelian surfaces: International Journal of Climatology, v. 19, p. 1267–1277, https://doi .org/10.1002/(SICI)1097-0088(199909)19:11<1267::AID-JOC418>3.0.CO;2-S.
- von Randow, C., Manzi, A.O., Kruijt, B., de Oliveira, P.J., Zanchi, F.B., Silva, R.L., Hodnett, M.G., Gash, J.H.C., Elbers, J.A., Waterloo, M.J., Cardoso, F.L., and Kabat, P., 2004, Comparative measurements and seasonal variations in energy and carbon exchange over forest and pasture in South West Amazonia: Theoretical and Applied Climatology, v. 78, p. 5–26, https://doi.org/10.1007/s00704-004-0041-z.
- Wallace, J.M., and Hobbs, P.V., 1977, Atmospheric Science: An Introductory Survey: New York, Academic Press, 467 p.
- Wallace, J.S., 1995, Calculating evaporation: Resistance to factors: Agricultural and Forest Meteorology, v. 73, p. 353–366, https://doi.org/10.1016/0168-1923(94)05084-J.
- Wang, H., and Liu, W., 2021, Soil temperature and brGDGTs along an elevation gradient on the northeastern Tibetan Plateau: A test of soil brGDGTs as a proxy for paleoelevation: Chemical Geology, v. 566, 120079, https://doi.org/10.1016/j.chemgeo.2021.120079.
- Wang, H., Liu, W., Zhang, C.L., Wang, Z., Wang, J., Liu, Z., and Dong, H., 2012, Distribution of glycerol dialkyl glycerol tetraethers in surface sediments of Lake Qinghai and surrounding soil: Organic Geochemistry, v. 47, p. 78–87, https://doi.org/10.1016/j.orggeochem.2012.03.008.
- Wang, H., Liu, W., and Lu, H., 2016, Appraisal of branched glycerol dialkyl glycerol tetraether–based indices for North China: Organic Geochemistry, v. 98, p. 118–130, https://doi.org/10.1016/j.orggeochem.2016.05.013.
- Wang, H., An, Z., Lu, H., Zhao, Z., and Liu, W., 2020, Calibrating bacterial tetraether distributions towards in situ soil temperature and application to a loess-paleosol sequence: Quaternary Science Reviews, v. 231, 106172, https://doi.org/10.1016/j.quascirev.2020.106172.
- Wang, H., Liu, W., He, Y., Zhou, A., Zhao, H., Liu, H., Cao, Y., Hu, J., Meng, B., Jiang, J., Kolpakova, M., Krivonogov, S., and Liu, Z., 2021, Salinity-controlled isomerization of lacustrine brGDGTs impacts the associated MBT'_{SME} terrestrial temperature index: Geochimica et Cosmochimica Acta, v. 305, p. 33–48, https://doi.org/10.1016/j.gca.2021.05.004.
- Wang, S., Yang, Y., Trishchenko, A.P., Barr, A.G., Black, T.A., and McCaughey, H., 2009, Modeling the response of canopy stomatal conductance to humidity: Journal of Hydrometeorology, v. 10, p. 521–532, https://doi.org/10.1175/2008JHM1050.1.
- Weber, Y., De Jonge, C., Rijpstra, W.I.C., Hopmans, E.C., Stadnitskaia, A., Schubert, C.J., Lehmann, M.F., Sinninghe Damsté, J.S., and Niemann, H., 2015, Identification and carbon isotope composition of a novel branched GDGT isomer in lake sediments: Evidence for lacustrine branched GDGT production: Geochimica et Cosmochimica Acta, v. 154, p. 118–129, https://doi.org/10.1016/j.gca.2015.01.032.

- Weijers, J.W.H., Schouten, S., van den Donker, J.C., Hopmans, E.C., and Sinninghe Damsté, J.S., 2007, Environmental controls on bacterial tetraether membrane lipid distribution in soils: Geochimica et Cosmochimica Acta, v. 71, p. 703–713, https://doi.org/10.1016/j.gca.2006.10.003.
- Wilson, K.B., and Baldocchi, D.D., 2000, Seasonal and interannual variability of energy fluxes over a broadleaved temperate deciduous forest in North America: Agricultural and Forest Meteorology, v. 100, p. 1–18, https://doi.org/10.1016/S0168-1923(99)00088-X.
- Wilson, K.B., Baldocchi, D.D., Aubinet, M., Berbigier, P., Bernhofer, C., Dolman, H., Falge, E., Field, C., Goldstein, A., Granier, A., Grelle, A., Halldor, T., Hollinger, D., Katul, G., Law, B.E., Lindroth, A., Meyers, T., Moncrieff, J., Monson, R., Oechel, W., Tenhunen, J., Valentini, R., Verma, S., Vesala, T., and Wofsy, S., 2002, Energy partitioning between latent and sensible heat flux
- during the warm season at FLUXNET sites: Water Resources Research, v. 38, 1294, https://doi.org/10.1029/2001WR000989.
- Wu, J., Guan, D., Han, S., Shi, T., Jin, C., Pei, T., and Yu, G., 2007, Energy budget above a temperate mixed forest in northeastern China: Hydrological Processes, v. 21, p. 2425–2434, https:// doi.org/10.1002/hvp.6395.
- Yue, P., Zhang, Q., Yang, Y., Zhang, L., Zhang, H., Hao, X., and Sun, X., 2018, Seasonal and inter-annual variability of the Bowen smith ratio over a semiarid grassland in the Chinese Loess Plateau: Agricultural and Forest Meteorology, v. 252, p. 99–108, https://doi.org/10.1016/j.agrformet.2018.01.006.
- Zhu, G., Lu, L., Su, Y., Wang, X., Cui, X., Ma, J., He, J., Zhang, K., and Li, C., 2014, Energy flux partitioning and evapotranspiration in a sub-alpine spruce forest ecosystem: Hydrological Processes, v. 28, p. 5093–5104, https://doi.org/10.1002/hyp.9995.